Surface Enhanced Raman Scattering of TNT on TiO_2 Substrates-Photodegradation Kinetics of Explosives

by

Edwin De La Cruz Montoya

A thesis submitted in partial fulfillment for requirement for the degree of

Master of Science in Chemistry

UNIVERSITY OF PUERTO RICO
MAYAGÜEZ CAMPUS
2007

Approved by:

_____	_____
Nairmen Mina-Camilde, Ph.D. Member, Graduate Committee	Date
_____	_____
Miguel E. Castro-Rosario, Ph.D. Member, Graduate Committee	Date
_____	_____
Samuel P. Hernández-Rivera, Ph.D. President, Graduate Committee	Date
_____	_____
Francis Patron, Ph.D. Chairperson of the Department	Date
_____	_____
Julio G. Briano-Peralta, Ph.D. Representative of Graduate Studies	Date

ABSTRACT

The majority of explosives found in antipersonnel and antitank landmines contain 2,4,6-trinitrotoluene (TNT). 2,4-Dinitrotoluene (DNT) is a common manufacturing byproduct in the synthesis and degradation of TNT. The production, testing and use of high explosives such as TNT and DNT, from the late 19th century to date has extensively contaminated soil and water at a large number of government installations. These high explosives are toxic and mutagenic and have been classified as environmental hazards and as priority pollutants by US EPA. For these reasons, the study of new processes for the detection and degradation of traces of these compounds is of world-wide interest. Nanotechnology is ideally suited to needs in these two areas by providing new materials and methods that can be employed for trace explosive detection and photodegradation. This work focused on modification of nanoscaled colloids of titanium dioxide (anatase), as substrates for use in Surface Enhanced Raman Scattering (SERS) spectroscopy and in photocatalytic degradation of explosives in water, a process assisted by luminous energy with wavelengths capable of electronically exciting a semiconductor.

Metallic oxides were found to give good Raman enhanced signals of target molecules. TNT increased the intensities of the Raman signatures for this technique and was evaluated for excitation sources of 488, 532, and 785 nm. Ultra fine particles of TiO_2 were generated by hydrothermally treatment of sol-gel derived hydrous oxide. SERS spectra of nanocrystalline anatase samples prepared with different average size: 38 nm (without acid), 24 nm (without acid), 7 nm (with HCl acid) and with KBr were obtained of mixtures with 0.5mg of TNT. The studies clearly indicated that the anatase crystal size affects the Raman signal of 0.5 mg of TNT.

The percentage decrease in TNT and DNT concentration, resulting from photocatalytic reactions conducted for 140 min, were 70% and 75%, respectively. The reaction rate was found to obey pseudo first order kinetics represented by the Langmuir-Hinshelwood model. Reaction rate constant of 1.67 [mg/L.min] (TNT) and 1.02 [mg/L.min] (DNT) were found.

RESUMEN

La mayoría de los explosivos encontrados en minas antipersonales y minas antitanques contienen 2,4,6-trinitrotolueno (TNT). Dinitrotoluenos (2,4 y 2,6-DNT) son comúnmente subproductos manufacturados en la síntesis y degradación del TNT. La producción, la prueba y el uso de explosivos altos, tales como TNT y DNT, a partir de fines del siglo XIX hasta la fecha han contaminado extensivamente el suelo y el agua en una gran cantidad de instalaciones del gobierno. Estos explosivos son tóxicos y mutágenos y clasificados como peligro para el medio ambiente y como agentes contaminadores de prioridad para la EPA. Por tal razón, el estudio de los nuevos procesos para la detección y la destrucción de los trazas de estos compuestos es un interés mundial. Nanotecnología es ideal a las necesidades en estas áreas proporcionando los nuevos materiales y métodos que se pueden emplear para la detección y la fotodegradación de trazas de explosivos. Este trabajo se centró en la modificación a nanoescala de coloides del dióxido titanio (anatasa), como substrato para uso en espectroscopia vibracional Raman realzada por superficie ("SERS") y la degradación fotocatalítica de explosivos en agua, proceso asistido por energía luminosa de longitudes de onda capaces de excitar electrónicamente un semiconductor.

Se encontró que óxidos metálicos dieron señales Raman aumentadas en las moléculas objeto de estudio. TNT aumentó las intensidades de las señales Raman para esta técnica y se evaluó para las fuentes de la excitación de 488, 532 y 785 nm. Partículas ultra finas de TiO_2 se generaron hidrotérmicamente tratando los óxidos acuosos derivados de geles. Los espectros SERS fueron adquiridos con nanopartículas de anatasa a diferentes tamaños de partícula 38 (sin acidificar), 24 (sin acidificar) y 7 nm (con HCl) y KBr mezclados con 0.5 mg de TNT. Los estudios indicaron claramente que el tamaño cristalino de anatasa afecta la señal de Raman de 0.5mg de TNT.

La disminución porcentual de la concentración de TNT y DNT, como resultado de reacciones fotocatalíticas conducidas por 140 minutos, fueron 70% y 75%, respectivamente. La rapidez de la reacción se encontró obedecer cinética de seudo primer orden, representada por el modelo de Langmuir-Hinshelwood. Se encontraron constantes de rapidez de reacción de 1.67 [mg/L.min] (TNT) y 1.02 [mg/L.min] (DNT).

To my Mother….

ACKNOWLEDGEMENTS

During the development of my graduate studies in the University of Puerto Rico, Mayagüez Campus, several persons and institutions collaborated directly and indirectly with my research. Without their support it would have been impossible for me to finish my work. That is why I wish to dedicate this section to recognize their support.

I want to start expressing an acknowledgement to my advisor, Dr. Samuel Hernandez Rivera because he gave me the opportunity to conduct research under his supervision. I want to express my gratefulness to another member of my thesis committee, Dr. Nairmen Mina-Camilde and Dr Miguel Castro for his support and collaboration in this work.

I would like to thank all my friends in Puerto Rico, for the shared moments, in special to my lab partners, Tatty, Marcia, Leonardo and Gabriel for their valuable collaboration in this work.

At last, but not least, I would like to thank my immediate family, my parents Wilson and Solangel, my aunt Maruja, my sister Esledy my brother Victor and my wife to be Andrea**,** for their unconditional support, inspiration and love.

TABLE OF CONTENTS

LIST OF FIGURES

LIST OF TABLES

APPENDICES

CHAPTER I

INTRODUCTION

Detection of trace amounts of explosive materials is an important task with a broad range of implications, from National Security and Defense to the cleanup of demilitarized installations. Nanotechnology is ideally suited to needs in these areas by providing new materials and methods that can be employed for trace explosive detection[1-2]. Surface chemistry methods that focus on modification of nanoscaled substrates for use in Surface Enhanced Raman Scattering (SERS) spectroscopy can take advantage of the commercialization of miniaturized spectrographs for trace explosive detection in a number of chemical environments. This work focused on studies aimed to the use of nanotechnology and surface chemistry for trace explosive detection. Explosive chemicals that were the focus of the work here included 2,4,6-trinitrotoluene, better known as TNT and 2,4-dinitrotoluene (2,4-DNT) and 2,6-DNT. The TNT molecule consists of three NO_2 groups bonded in the para and in both ortho positions with respect to the methyl group in toluene[3]. Demonstrating SERS phenomenon of TNT on TiO_2 particles and its colloidal suspension was the primary objective of this research.

Post manufacturing and disposal practices of explosives have resulted in contamination of soil and groundwater by this toxic nitroaromatic compound[4]. In recent years the remediation of TNT-contaminated sites has been recognized as a challenging environmental problem, and several remediation strategies have been implemented with varying degrees of success. Removal of TNT from water by adsorption onto activated charcoal is a proven technology, but it suffers from problems associated with the regeneration of the substrate and the ultimate disposal of the solid adsorbent. Biological treatment[5-6] or direct solar photolysis[7-8] of TNT results in complex mixtures of products, the identities and toxicities of which are not entirely known.

For theses reasons, the study of new oxidation processes for the degradation of nitroaromatic explosives is of utmost importance. One of the most relevant investigations is the application of solar energy in the photodegradation of organic compound. In photocatalysis, degradation is provided by luminous energy, with wavelengths that are

capable of exciting a semiconductor (catalyst), generally a metallic oxide, to the degree that makes the material behave as a conductor on the surface or interfacial region between solid and the solution, in which the oxidization-reduction reaction develops. The photocatalytic treatment of water with TiO_2 is efficient for the destruction of many organic pollutants. The focus of this work is to determine the possibility of applying the TiO_2 photocatalytic reaction to the treatment of TNT and DNT contaminated water.

Chapter II

THEORY

2.1 Explosives

An explosive is a material, either a single substance or a mixture of substances, which is capable of producing an explosion by its energy released. Explosives can be classified by their performance and uses: primary explosives (or low explosives) undergo a very rapid transition from burning to detonation. They can transmit the detonation to less sensitive explosives. They can be detonated by heat or shock. Example of explosives primary is mercury fulminate and lead azide. Secondary explosives (or high explosive) cannot be detonated readily by heat or shock, and they are less sensitive than primary explosives, they need the later for detonation. Examples of secondary explosives are: TNT, RDX, PETN and DNT [9].

Figure 1 shows TNT molecule, the first, and most important (as far as quantity of production goes) of the monosubstituted TNBs. TNT is soluble in benzene, toluene, and acetone. It is slightly soluble in alcohol and virtually insoluble in water. Because of its moderated melting point (approximately 80°C) and the fact that it does not decompose upon melting, it is used most often in melt-cast form.

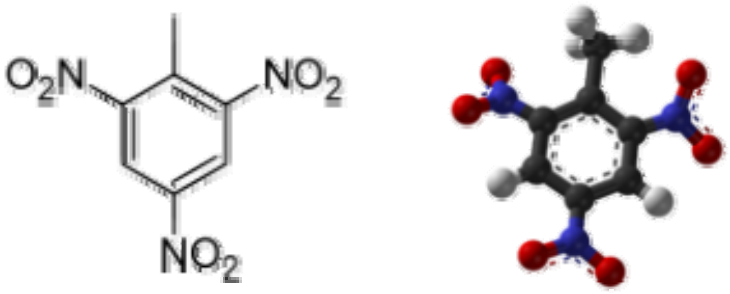

(a) (b)

Figure 1: Chemical structure of TNT: (a) Lewis representation; (b) “ball and sticks” model.

TNT is produced, by direct nitration with nitric and sulfuric acids. The synthesis is done in a stepwise procedure. First toluene is nitrated with a mixture of sulfuric and nitric acid. Even lower-concentration acid mixtures are capable of doing the first and second introduction of

nitro group. The nitro groups decrease the reactivity of the toluene drastically because they are electron-withdrawing groups. After separation, the mono- and dinitrotoluene is fully nitrated with a mixture of nitric acid and oleum (sulfuric acid with up to 60% dissolved SO_3). This mixture is far more reactive and is capable of introducing the last nitro group.

Some of the explosives that that constitute secondary components of landmines are 1-methyl-2,4-dinitrobenzene, and 1-methyl-2,6-dinitrobenzene better known as 2,4- and 2,6-DNT. These two compounds are manufactured by denigration of toluene or by mononitration of p-nitrotoluene. Mononitration of o-nitrotoluene leads to a 1:2 mixture of 2,4- and 2,6-DNT. When explosives come in contact with soil, humidity, at various pH and under the action of UV radiation they experiment reactions that change the characteristic signatures. DNT, shown in Figure 2, is one of the main explosives used in the production of landmines and is a product of degradation and an impurity in the synthesis of TNT[10]. It occurs in approximately 80 percent of all mines. Explosives that are based on TNT contain by-products, primarily impurities and degradation products such as dinitrobenzene (DNB) and DNT.

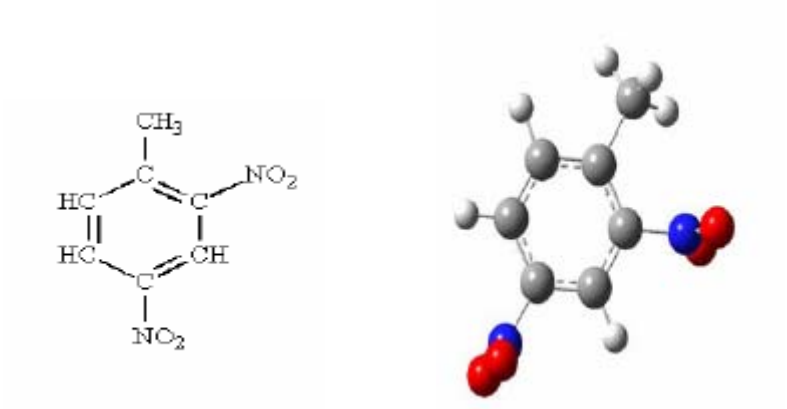

(a) (b)

Figure 2: Chemical structure of DNT: (a) Lewis representation; (b) "ball and sticks" model.

2.2 Raman spectroscopy

The phenomenon known as the Raman Effect was first described by the Indian physicist Chandrasekhar Venkata Raman in 1928, which make him deserve the "Nobel" of physics in 1930. Raman gave the name to the inelastic phenomenon of light dispersion that permits

the study of the rotational and vibrational modes of molecules. In 1923, while Raman and his student Krishnan studied the dispersion of light in water and in purified alcohols, observed a change in color in a sunlight ray when it was filtered and their equipment could not eliminate this effect. They suspected that the phenomenon was a characteristic property of the substance examined. For the next five years they made various experiments published their famous article in *Nature* in 1928, in which they described this new type of secondary radiation[11].

Raman spectroscopy is a technique that provides chemical and structural information of almost all materials, organic and inorganic compounds, allowing for their identification in few seconds. Analysis by means of spectroscopy Raman is based on examining the scattering of monochromatic light by a material[12]. Only a small portion of the light is dispersed inelastically, experimenting slight changes with respect of the incident light frequency which are characteristic of the analyzed material. The analysis by Raman spectroscopy is based in passing a beam of monochromatic light of frequency $\boldsymbol{\nu_0}$ through a sample whose molecular characteristics are unknown, and examining the dispersed light by the sample. The majority of the dispersed light presents the same frequency that the incident light but a really small fraction presents a change in frequency, result of the interaction of light with the matter. The light that maintains the same frequency $\boldsymbol{\nu_0}$ of the incident light is known as Rayleigh dispersion and does convey any structural or chemical information of the molecular composition of the sample. Dispersed Raman light in which the incident frequency changes is the one known as Raman dispersion. The new frequencies are $\boldsymbol{\nu_0 + \nu_R}$ and $\boldsymbol{\nu_0 - \nu_R}$ are the Raman frequencies that are characteristic of the chemical nature and the physical state of the sample and are independent of the incident radiation.

The variation of observed dispersed Raman frequencies, are the equivalent to observation of energy variations in molecules[13]. The atoms chemical bound to form molecules and crystalline networks, are exposed to constant vibrational and rotational movements. These patterns occur at very determined frequencies which are functions of the masses of the particles that participate and the dynamic behavior of the bonds. At each vibrational and rotational movement of a molecule corresponds to a determined value in molecular energy. Figure 3 shows an energetic diagram in which each state of energy is represented by a horizontal line.

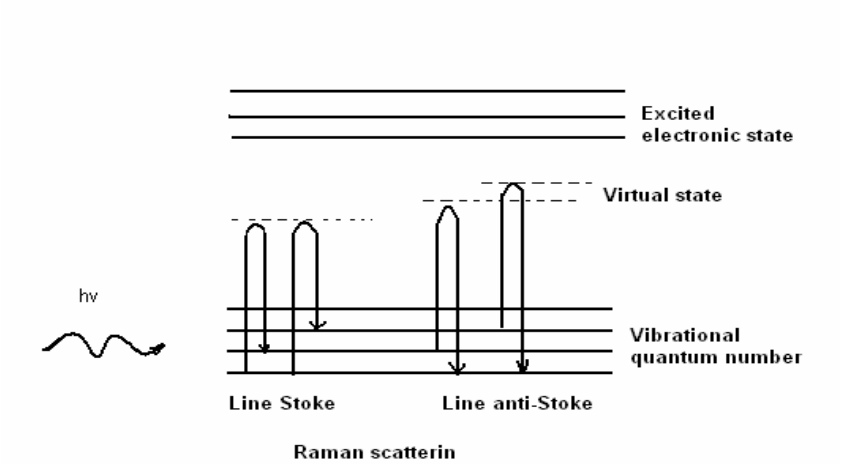

Figure 3: Energetic diagram in which horizontal lines represent different vibrational states and show the transitions between energetic states excited with monochromatic light (ν_0).

When photons of the monochromatic incident light beam hit the target molecules, with energy $h\nu_0$ larger than the difference in energy between two vibrational levels of a molecule, the majority of the light photons go through unaltered, but a small fraction is dispersed. This dispersion can be interpreted as the following process: the photon collision takes the molecule to a not allowed transitory higher electronic energy level which the molecule abandons quickly to end in one of the allowed vibrational energy levels on the ground electronic state, emitting a photon. The frequency of the emitted photon depends on the energetic transition made by the molecule. The following cases can be distinguished:

- If the result of the molecule-photon interaction is a dispersed photon of the same frequency as the incident photon, it is said that the collision is elastic and that neither the photon nor the molecule suffers variation in its energetic state. The molecule goes to the same energy level that it had before the collision and the dispersed photon has the same frequency ν_0 that the incident, giving as a result Rayleigh dispersion.
- If the result of the molecule-photon interaction is a dispersed photon of a different frequency with respect of the incident photon, it is said that the collision is inelastic. In this case two phenomena can been seen:

1. if the dispersed photon has a lower frequency than the incident photon, an energy transference from the photon to the target molecule occurs. The photon is dispersed with frequency ν_0-ν_R and Raman Stokes dispersion is produced.
2. if the dispersed photon has a higher frequency than the incident photon an energy transference from the molecule to the photon has occurred. This means that the molecule was not in its fundamental vibrational state before the collision. The photon is dispersed with frequency $\nu_0 + \nu_R$ and the Raman dispersion is termed anti-Stokes.

Each material will have a series of values of ν_R characteristic of its polyatomic structure and the nature of the chemical bond that forms it. The Raman spectrum represents this phenomenon by a plot of the dispersed intensity as a function of the number of waves per cm or wavenumber. The wavenumber is a proportional magnitude to the frequency and inversely proportional to the wavelength. That is expressed in cm^{-1}:

$$V = \nu / c = 1/\lambda \ [cm^{-1}]$$

2.3 Surface-Enhanced Raman Spectroscopy

In 1978 Fleischmann and Albrecht and Jeanmarie and van Duyne discovered that pyridine molecules adsorbed on a silver electrode experience an enhanced Raman spectrum that was a million fold more intense than expected. This effect was given the name Surface Enhanced Raman Scattering (SERS)[14]. Since then the effect has been demonstrated with many molecules and a number of metals, including Cu, Ag, Au, Li, Na, K, Pt, and Rh. The field developed aggressively, even explosively, for the first decade or so and then settled down a bit as it entered its teenage years. Interest shifted from fundamental studies to applications and a steady stream of papers was published in diverse fields which included electrochemistry, analytical chemistry, chemical physics, solid state physics, biophysics and even medicine.

The effect is based in the enhancement of the inelastic dispersion originated from determined molecules in presence of a specially prepared roughened metallic nanostructure, which increases the intensity of selected molecular vibrations by a factor exceeding 10^5 – 10^6. The cause of the extraordinary enhancement of the Raman dispersion in presence of

metallic nanostructures is still in discussion. The majority of the works done in laboratory explain the nature of the phenomenon by considering two fundamental models:

a) The electromagnetic model (EM)
b) The charge transference or chemical model (CTM)

All the experimental indication found until today, points to consider that both occur simultaneously, even though there is not a definite agreement of the contribution of each one of them in the factor of total intensification[15].

2.4 Catalysis

Numerous investigators assign catalysis a prominent place in the development of new benign chemical process with the environment. In the literature that concerns to the theme, it is often spoken in terms of *ideal catalyst* and *ideal recoverable catalyst* making reference to catalyst capable of to take place more efficient and selective reactions that permits to eliminate sub-product and other remainder compound of the conventional reactions and can be recovered from the middle of the reaction to be reused.[16] In addition, this ideal catalyst permits lower energy consumption. The applied field of catalysis covers the prevention and reduction of contamination by the elaboration of new catalytic cleaner routes. With respect to the *elaboration of clean catalytic routes*, multiple examples exist in the literature recently found, in which few of the mention objective are fulfilled in relation to the ideal catalyst and to the principle of green chemistry. In general, certain tendencies exist to hydrogenise the homogenous catalyst. It deals with combining the advantages of the homogenous catalyst with the recuperation facility and of the recycled heterogeneous catalysts.[17-18]

It's described, for example, the use of metallic complex immobilized over rough silica, which can participate in very selective reactions and can be easily recovered and reused. Zeolites also possesses a high potential in the benign environmental synthesis, because their chemical modification allow for selective reactions to occur. It has also been described for this catalysts its reuses without a loss in its activity. The biocatalysis has also been demonstrated to be a very useful technology for chemical industries. In some cases it has permitted reactions that can not be easily done from the classic organic chemistry, and in other case, has allowed very selective reactions that can replace various chemical levels. A

last example of clean catalytic routes, for synthesis compounds, consists in the use of oxides and metallic hydroxides to make oxidation reactions at normal temperature, with rise-up yield and the recuperation of the catalyst.

The heterogenic catalysts permits the degradation, and inclusive the mineralization, of recalcitrant organics pollutants present in the water or in the air, basically by the use of an semiconductor, an irradiation source and presence of oxygen in the middle of the reaction.

TiO_2 is an innocuous semiconductor that operates at environment temperature, under ultraviolet light, in a clean way, and doesn't exhaust its photo reactivity[19-20]

2.5 Heterogeneous photocatalysis

The term photocatalysis was introduced to the science glossary in 1930. When it is spoken about photocatalysis, reference is made to a catalytic reaction that involves the absorption of light by a catalyst or a substrate. One of the application of the photocatalysis, like it have been told, is found in the resolution of problems of environmental interest, like it can be the depuration of water or air, using a semiconductor sensible to light as a catalyst. In this case we talk about heterogenic photocatalysis because the photoreaction occurs in the surface of the catalyst (in the liquid-solid or gas-solid interface respectively). The heterogenic photocatalysis allows the degradation and mineralization, of a big variety of organic compounds as the global reaction goes:

$$\text{Organic pollutant} + O_2 \xrightarrow[h\nu]{\text{semiconductor}} CO_2 + H_2O + \text{minerals acid}$$

The initial stage of the process consists in the production of electron hole pairs in the semiconductor particles. When a photon with an energy that equals or is larger than the energy of the jump of the semiconductors band E_g, an electron is promoted from the valence band (VB) to the conduction band (CB), generating a hole, h^+, in this last band[21-22].

$$\text{Semiconductor} \xrightarrow{h\nu} (e^-, h^+)$$

The electrons that reach the conduction band can move inside the semiconductor network. Also it will also move to free space that has been left in the valence band. As shown in

figure 4, the electrons and the photogenerated holes can follow different ways. By a side, both species can migrate to the semiconductor and jumble in *electronic transference* with absorbed species in the surface of the particle, even though they are organic species, inorganic or the same solvent. The electron reduces an electron acceptor, A, absorbed in the semiconductor surface as it shows way *a*. At the same time, the hole can accept an electron of a specie D giver of electron, in a way that this specie oxide (way b) the reactions that take place are the followings:

$$e^- + A \longrightarrow A^-$$

$$h^+ + D \longrightarrow D^+$$

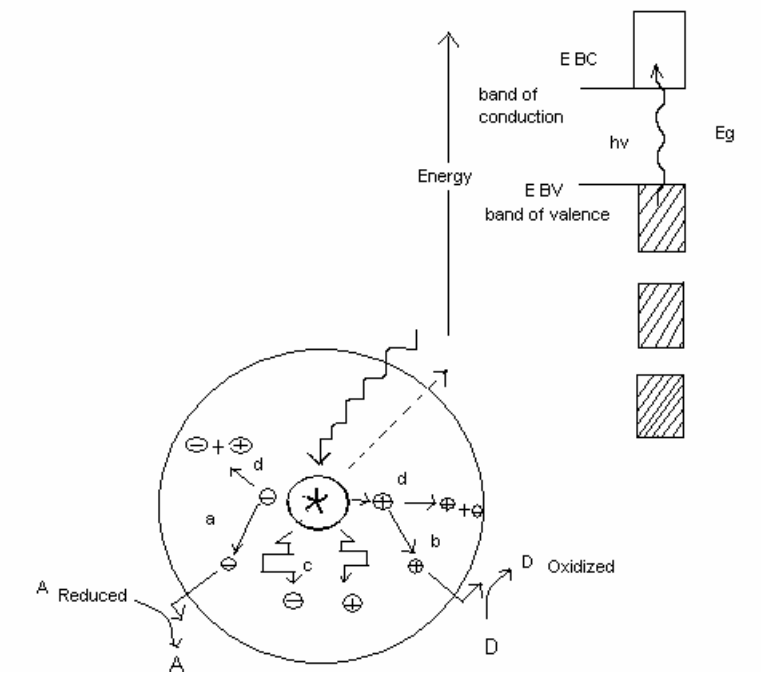

Figure 4: Main processes that occur in a semiconductor particle after electronic excitation. On the surface, the photodegenerated electrons can reduce to an electron acceptor (a) and the photodegenerated hollows can oxidize to an electron donor (b). The electron-hollow recombination can take place inside the particle (c) or at the surface (d).

Therefore, the capture of an electron by part of a species A generates a radical anion A^-, meanwhile the capture of an hole by part of a specie D generates a cation radical D^+. These radical ions are very reactive and can react among them and with other absorbents, and

inclusive they can be made from the semiconductor surface into the interior of the solution and participates in a chemical reaction in the sine of the aqueous phase[23].

The thermodynamics requisite for the electronic interfacial transference are schematically shown in Figure 5. The photo induced reduction is thermodynamically permitted for molecules with a reduction potential less negative that the limit of the conduction band of the semiconductor (except if kinetic limitations exist). By similar consideration, the photo induced oxidation can occur to any molecule that posses a less positive oxidation potential that the limit of the valence band of the semiconductor, always that the velocity of the cation radical formation is competitive from the kinetic point with the other process shown in Figure 5. Several process that influence the interfacial electronic transference, such as the variation of the electrochemical potential of the two phases to reach the balance, the formation of the level of space charge and the bending of the valence and conduction band of the semiconductor that occurs when this one are found in a electrolyte solution that contains a redox pair.

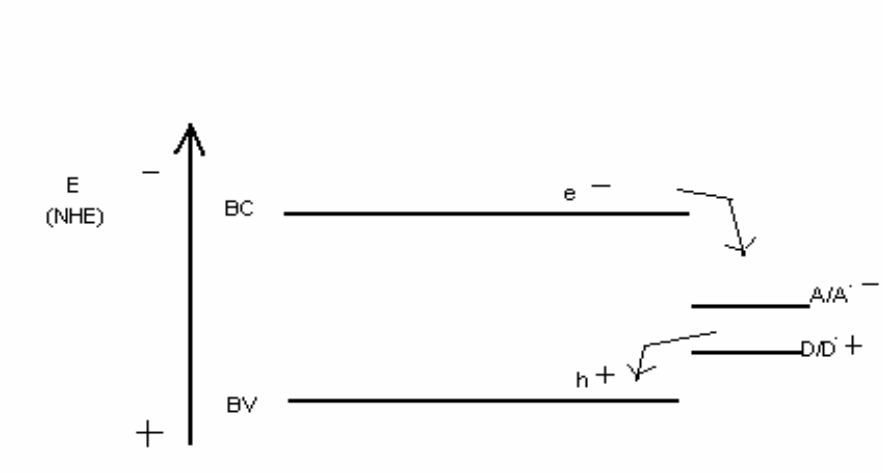

Figure 5: Thermodynamic requirement for the interface electronic transference in the semiconductor illuminated surface.

In competition with the interfacial electronic transference process it is found, the *electron-hole recombination*. The recombination can occur in the interior of the semiconductor particle like in the surface, and comes accompanied by the liberation of heat[24]. We should point that the recombination is detrimental for the efficiency of the photocatalysis process, given that reduces the number of electrons and holes that can be transferred to the absorbed species in the semiconductors surface. Avoiding this process constitutes an important area

of investigations in the heterogenic photocatalysis and for other semiconductors applications. Ahead some strategies are commented that actually investigates to avoid this process. In the present investigations it has been worked with semiconductor, titanium dioxide (TiO_2).[25]

2.6 Titanium oxides (TiO_2) characteristics

Lots of simple semiconductor, like oxides and sulfides, are adequate to catalyze an ample range of chemical reactions. Some of these semiconductors that can be used as photocatalyzers, are those shown in Figure 6 from all of them, TiO_2 is, for various motives, the semiconductor most used for environmental applications. In first place, a lot of organic compounds have the potential of oxidation over the valence band of the TiO_2 and for these motives they can be oxidized photo catalytically by the TiO_2. In second place, the redox potential of the pair H_2O / OH ($OH + e^- \longrightarrow OH^-$) it's found inside the domain of the band jump of the material. These done, like seen ahead, haves an special interest. Others motive for the great use is the TiO_2 is its chemical stability in front of acids bases and strong acids and it stability under illumination, for last the TiO_2 is chemically cheap[26].

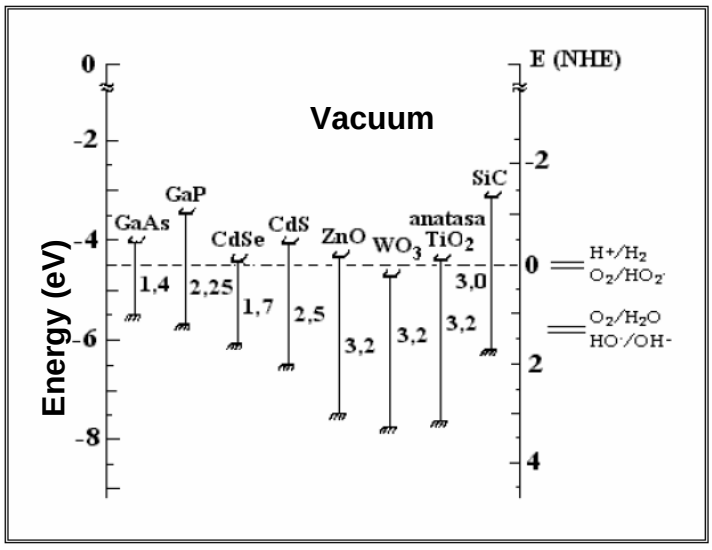

Figure 6: Band potentials of different semiconductors in aqueous electrolytes at pH = 1.[27]

Other semiconductors with photocatalytic activities, like zinc oxide, cadmium sulfur and the iron oxides, are not stable in all the pH range and suffer photo corrosion. With respect

to ZnO, even though it has band limits position very similar to the TiO_2, suffers photo corrosion induced by auto oxidation, that gives a place to the formation of $Zn(OH)_2$ in surface of the particles of ZnO and the appearance of Zn^{2+} in solution, which finishes conducting to the inactivation of the catalyst. In the other side the CdS and iron oxides, in spite of having an adequate spectral answer for the pick up of solar radiation, they are also not appropriate, because the CdS discomposes giving place to soluble species of Cd^{2+}, environmentally injurious and the iron oxides also suffers corrosion[28].

In spite of spectral answer of the TiO_2, fits to mention that this material is only active in the near ultraviolet region (UVA) had that its bands jump is found between 3.02 and 3.23 eV, according to its crystalline structure, is respectively, rutile or anatase. For this motive, TiO_2 can only use about 5% the intensity of the solar light spectrum that is the part that corresponds to the ultraviolet range that is found less than 400 nm, like Figure 7.

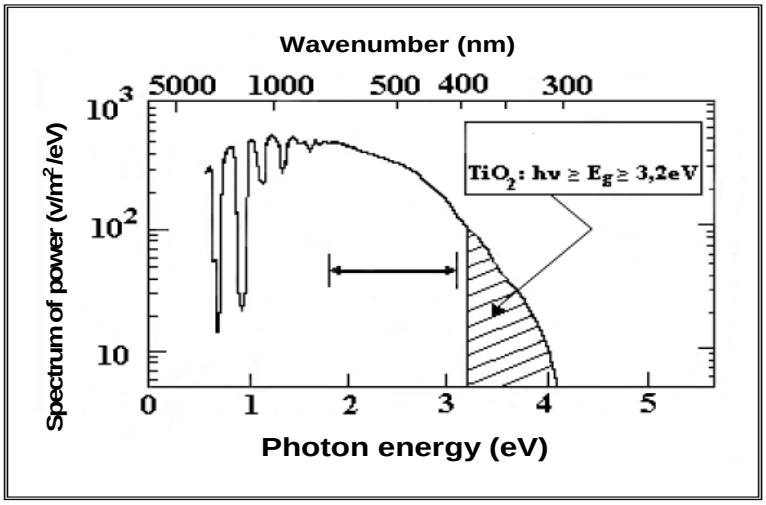

Figure 7: Spectrum of solar radiation. The SiO_2 is active in the lined zone (below 400 nm), that corresponds to a 5% of intensity of the Spectrum of solar radiation[29].

The most thermodynamically stable crystalline TiO_2 structure is the rutile. Nevertheless the structure that presents the mayor photo catalytic activity is the anatase that is used in a habitual way for environmental decontamination applications. Both structures can be described in terms of TiO_6 octahedral chains being the difference among them the distortion of each octahedral and the union pattern of chains: in the structure of rutile each octahedral is with contact with ten vicinal octahedral meanwhile in the anatase structure each octahedral is in contact with eight vicinal. Like a consequence of this difference in the

structures network, the rutile and anatase has mass densities and electronic band structure, very different[30].

The surface particles of metallic oxides can be acidic or basic. In the case of TiO_2, the principal functional group is the *titanol* ~ TiOH. The hydroxide groups of the TiO_2 surface present the following acid-base equilibrium:

$$TiOH_2^+ \xrightarrow{K_{a\,1}} TiOH + H^+$$

$$TiOH \xrightarrow{K_{a\,2}} TiO^- + H^+$$

Where K_{a1} is the acidity constant of the first acid dissociation and K_{a2} is the acidity constant of the second disassociation. The pH of the zero point charge, pH_{zpc}, comes given by the half of the sum of the superficial pK_a.

$$pH_{zpc} = ½ (pKa_1 + pK_{a\,2})$$

Chapter III
PREVIOUS WORK

Raman Spectroscopy is an established tool for vibrational spectroscopy analysis and can be used in Point Detection mode to detect explosive components of landmines. Interactions of explosives with different substrates can be measured by using quantitative vibrational signal shift information of scattered Raman light associated with these interactions. Ideally, vibrational spectroscopic techniques have the potential to remove false positives, since every chemical has a unique bond structure. The capabilities of surface-enhanced Raman spectroscopy to detect the chemical vapor signature emanating from buried TNT-based landmines. Silvia et al. presented reproducible results obtained from blind tests controlled by the Defense Advanced Research Projects Agency (DARPA) that demonstrated vapor detection of 2,4-dinitrotoluene at concentration levels of 5 ppb or less. The results presented used acquisition times of 30 s on a field able system and showed that SERS could be a significant improvement over existing landmine detection methods[30-32].

The characterization of explosives by Raman spectroscopy was used to investigate the processes involved in nitration reaction. The Raman spectrum of RDX was recorded using 632 nm excitation by Kniepp et al. The important –N-NO_2 vibrations are observed at 1312cm^{-1} (symmetric NO_2 stretch), 1597cm^{-1} (asymmetric NO_2 stretch) and 885cm^{-1} (N-N stretch). Also has used FT-Raman with NIR excitation to demonstrate the discrimination of two of the major components in Semtex, RDX and PETN[33]. Different batches of Semtex could be differentiated on the basis of the content of each of these two compounds. They also demonstrated the analysis of RDX and PETN using visible lasers and they confirmed that the in-situ detection of explosives was both feasible and practical. It was show that explosive samples 1um^3 in volume (1fL) or 1 picogram in mass could be identified from fingerprints[33]. They have reported the sensitive detection of TNT using SERS. TNT of concentration 10^{-7} M was adsorbed on to colloidal gold and silver in aqueous solutions and SERS spectra were observed using NIR excitation. Due to a lack of sensitivity however, the vapors detection of TNT was not possible under these conditions.[33] The detection of TNT by Raman spectroscopy is well documented and is relatively easy to obtain highly resolved Raman spectra of TNT crystal in a short period of time. The spectrum was recorded using

632 nm excitation and shows the import $ArNO_2$ vibrations at 1369 cm^{-1} (symmetric NO_2 stretch), 1542 cm^{-1} (asymmetric NO_2 stretch) and 829 cm^{-} (NO_2 bend).

Titania has been extensively used in a variety of applications such as gas sensors, dielectric ceramics, catalysts for thermal or photoinduced processes, photovoltaic solar cells, and pigments. The physical and chemical characteristics of TiO_2 can be controlled by its particle size, morphology, and crystalline phase. Nanostructure materials with ultra fine crystallite sizes (<100 nm) and high surface areas have attracted substantial interests due to their unusual optical, electrical, and SERS[28]. It is important that hydrothermally obtained powders could be produced with a different microstructure, morphology and phase composition by varying parameters such as temperature, pressure, duration of the process, concentration of chemical species, concentration of a solute and pH of solutions. In the literature about hydrothermal synthesis of nanocrystalline titanium dioxide the main attention is paid to the hydrothermal treatment of $TiO_2.nH_2O$ amorphous gels. At the same time, information about nanocrystalline Titania derived from high-temperature hydrolysis of aqueous solutions of titanium salts at temperatures above 100 °C is almost missing.[35] Nanocrystalline TiO_2 materials have been successfully synthesized via sol-gel hydrolysis precipitation, followed by calcinations or hydrothermal treatment. High water: alkoxide ratios were found to favor the formation of ultra fine Titania particles. Anatase grains as small as 6 nm were obtained via hydrothermal treatment at 80 °C, without the grain growth or particle agglomeration commonly induced by the calcinations process. Ten nanometer sized anatase nanocrystals derived via hydrothermal aging at 180 °C were shown to possess unusual thermal stability against grain growth and the anatase-rutile phase transformation. Rutile grains have been generated with ultra fine grain size via hydrothermal processing at 180° underwent neither phase change significant grain growth up to 800°C.

Nanocrystalline rutile TiO_2 particles have also been attained via hydrothermal treatment in an acidic medium. They possessed an ultra fine rutile grain size and a high surface area, which could not be achieved via phase transformation from thermal treatment of anatase particles. Hydrothermal synthesis of TiO_2 colloids is based on hydrolysis and pressure treatment of titanium isopropoxide precursor in acidic solutions. The influence of the use of

nitric and acetic acids during synthesis was studied, showing a significant effect on the colloids crystal structure. Colloids that were prepared in acetic contain more of the {101} structure face in comparison with the colloids prepared in nitric acid.[36]

Chapter IV

SERS of TNT on TiO_2 Substrates

4.1 METHODOLOGY

4.1.1 Reagents and Instruments

Crystalline samples of TNT used for the experiments described here were purchased from Chem. Service Inc., West Chester, PA (crystals, 98%, 30% water). Titanium (IV) oxide used was acquired from Aldrich Chemical Company, Inc. Milwaukee, WI, catalog number: 1317-70-0. Titanium (IV) oxide puratronic, 99.995% mixture of phases, predominantly rutile and anatase CAS # 13463-67-7 were acquired from Strem Chemicals, Inc., Newburyport, MA.

Renishaw Raman Microscope RM2000 system was employed for vibrational spectroscopy measurements. This system was equipped with a Leica microscope. A Coherent, Inc. INNOVA 308 argon ion laser system operating at 488 and 514.5 nm laser lines was employed as excitation source. The other excitation sources were a diode pumped 532 nm green laser with an variable output power up to 1 W was a Millennia II laser (Spectra Physics) and a Renishaw High Power 785 nm diode laser (200 mW maximum power). The laser beams were focused onto gold slides through objectives with 5x, 10x, 20x and 50x magnifications. The spectra were obtained in the 100-3800 cm^{-1} range. Integration time used was 10 seconds and three acquisitions. A nominal 1 cm^{-1} resolution was maintained in order to look for small changes in the Raman Shift spectra.

4.1.2 Measurements

Several experiments were carried out to observe the enhancement of the Raman signatures of TNT with TiO_2. In these experiments TiO_2 was used in the rutile and anatase phases and included depositing finely divided particles, in order to increase the surface area of the substrate. Anatase was converted to rutile by heating in a furnace slightly higher than the phase transition temperature for several minutes. Upon examination of the Raman spectra of both sources of TiO_2 it was confirmed that the conversion was not 100% effective.

4.1.3 Effect of the phases different of Titanium in Raman spectra of TNT

In these experiments TiO_2, in the rutile and anatase phases, was used for the SERS experiments. Mixtures of 0.5, 1.0, and 1.5 mg of TNT and 10 mg of TiO_2 were finely ground, compacted and deposited on stainless steel surfaces. Raman Shift spectra at different regions of the surfaces were acquired using the 532 nm laser source using 0.17 W and 10 s of integration time. The spectra were recorded in a Renishaw Raman Microspectrometer.

4.1.4 Raman Spectra of traces of TNT deposited on metal/TiO_2 Substrates

Traces of TNT were deposited on SS slides using Thermal Inkjet Technology (Hewlett-Packard, Aguadilla, PR). Raman Spectra of traces of TNT deposited on the metal substrates were recorded using 532 nm laser source. TiO_2 was scattered on traces of TNT and Raman spectra were recorded.

4.1.5 Raman spectra of TNT mixture Anatase-Rutile in different compositions

Measurements of Raman spectra of 1.0μL of TNT $1x10^{-2}$ M deposited on tablets of anatase-rutile mixtures prepared in different proportions: 20-80%, 40-60%, 60-40%, 70-30%, 80-20%, 100-0%, and KBr. The objective of this experiment was to determine the influence of the presence of the two phases of titanium dioxide on the TNT Raman Shift spectrum.

4.1.7 Raman Spectra of TNT on Nanocrystalline Anatase

SERS spectra of TNT were obtained for the analyte deposited on nanocrystalline anatase samples. TiO_2 nanoparticles prepared at different sizes: (without acid) 38 nm, (without acid) 24 nm, (with HCl acid) 7 nm were used to observe enhanced Raman spectra of 0.5mg of TNT. KBr mixture with 0.5mg of TNT was used as control. These particles sizes were characterized with X-ray diffraction (XRD) and Raman.

4.1.7.1 Synthesis of Anatase Nanocrystals

TiO_2 nanocrystals were derived via sol-gel hydrolysis precipitation of titanium isopropoxide (Ti $(OC_3H_7)_4$), followed by calcinations treatment. A specific amount of

titanium isopropoxide was dissolved in anhydrous isopropanol and mixed with a water isopropanol solution with water: alkoxide molar ratio of 3.3 and 25. Isopropoxide solutions were added drop wise to the aqueous solutions with vigorous stirring at room temperature. White precipitate of hydrous oxides were produced instantly, and the mixtures were stirred for at least 2h. The resulting materials were then dried and the amorphous precipitates were then subjected to hydrothermal treatment.

4.1.7.2 Characterization

Titania samples were characterized by powder X-ray diffraction (XRD) with a Siemens D5000 diffractometer (45 kV, 40 mA) using Ni-filtered Cu-Kα radiation (λ = 1.5406 Å). XRD patterns were obtained for 20-70° (2θ) by step-scanning with a step size of 0.02°. To determine the average crystallite size, peak broadening analysis was applied to anatase (101) diffractions using Scherer's equation. The samples were also characterized by Raman spectra in order to determine the phase anatasa, and the absorption spectra of the aqueous TiO_2 nanoparticle dispersion.

4.1.8 Raman Spectra of TNT on Colloidal Suspensions of TiO_2

Several experiments were carried out to observe the enhancement of the Raman signatures of solution of $1x10^{-3}$ M TNT. Spectra of TNT with TiO_2 colloid (25 nm) at different pH values: 2.4, 4.3, 7.2, 3.3, 10.9 and 12.3 were measured. In addition, spectra of TNT with TiO_2 colloid A (15 nm) at pH: 7.2 at different acquisition times: 10, 20, 30, 40, and 60 s were taken. Latterly spectra of TNT of $1x10^{-3}$ M with TiO_2 colloid A at pH: 7.2 to 60 s of acquisition were acquired at different ratios TNT/colloid: 100 μL/800 μL, 200 μL/600 μL, and 300 μL/600 μL respectively. Spectra of $1x10^{-3}$ M TNT with TiO_2 colloid B (40 nm) were recorded at 10 s of acquisition at different pH: (a) 2.4, (b) 3.3, (c) 11.0, (d) 12.4, (e) 7.2, (f) 11.8 and neat TNT.

4.1.9 Synthesis of Ag-TiO_2.

The preparation of Ag/TiO_2 nanoparticles can be considered as a combination of two processes that occur sequentially in a single mixture reaction, the formation of the silver core and the coating. The starting reaction mixture is prepared from two solutions. The first

solution contains equimolar amounts of isopropoxide and isopropanol in water in a concentration approximated of 5.75mM for each of both components.

The second solution is 2.8 mM $AgNO_3$ in citrate of sodium. Freshly prepared 20 mL of the first solution and 5 mL of the second were mixed in a round bottom flask and stirred while heating at a reflux temperature. After 90 minutes the colloids attained a dark green coloration.

4.1.10 Raman Spectra of TNT on Colloids of Ag/TiO_2

The objective of this experiment was determined influence of the pH on enhancement of the Raman signatures of solution of TNT. Later were carried out to observe the enhancement of the Raman signatures of solution of $1x10^{-3}$ M, $1x10^{-4}$ M, $1x10^{-6}$M and $1x10^{-8}$M of TNT with the best pH observed. Aliquots of 100 μL of $1x10^{-3}$ M TNT solution at different pH were deposited in 800 μL of colloid Ag/TiO_2 with 100 μL of sodium citrate and then deposited in capillary tubes. Raman Spectra were recorded with different excitation wavelengths: 532 nm (green), 785 nm (red), 488 nm (blue). Moreover, Raman measurements were also done in portable Raman spectrometers of excitation wavelengths 532 and 785 nm.

4.2 RESULTS AND DISCUSSION

4.2.1 Effect of the phases different of Titanium in Raman spectra of TNT and TNT deposited on the metal

Figure 8 shows the collection of spectrum SERS of TNT obtained with oxide of titanium IV it mixture with greater % of the form rutile in concentration of 2.0, 1.0, and 0.5mg which are compared with the spectrum non-SERS. An increase in the intensity of the signal is observed being but strong for the spectrum of greater concentration, in individual for the band of 1359 cm^{-1} characteristic of the group nitro. The calculated areas of this tip are of $6.5x10^6$, $4.5x10^6$, 254738 and 162533 respectively. The determination of the magnitude of the area Raman enhanced provides a quantitative measurement to us with a rate of 40, 27 and 15. The increases of intensity due to the spectrum where used the mixture can be seen in figure 9 whose corresponding areas to the tip of the group nitro are $1.32x10^6$, $1.24x10^6$ for the concentration of 1.0mg and 0.5mg of the TNT.

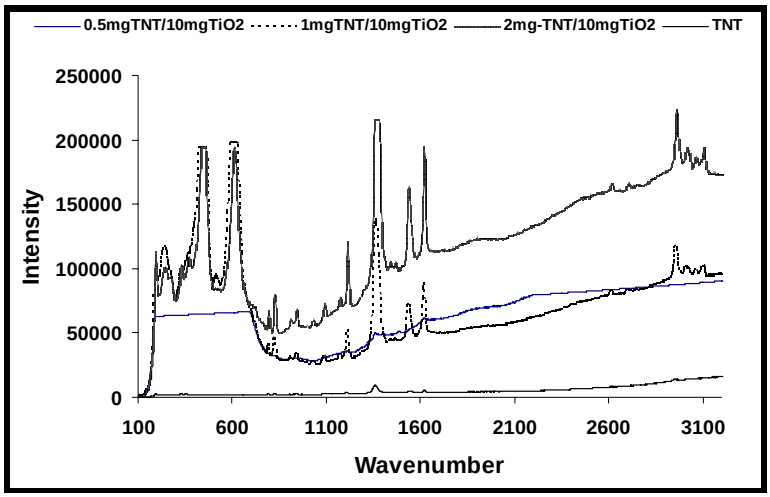

Figure 8: Different proportions of TNT and TiO_2 for different Mixtures of rutile and anatase: high rutile percent.

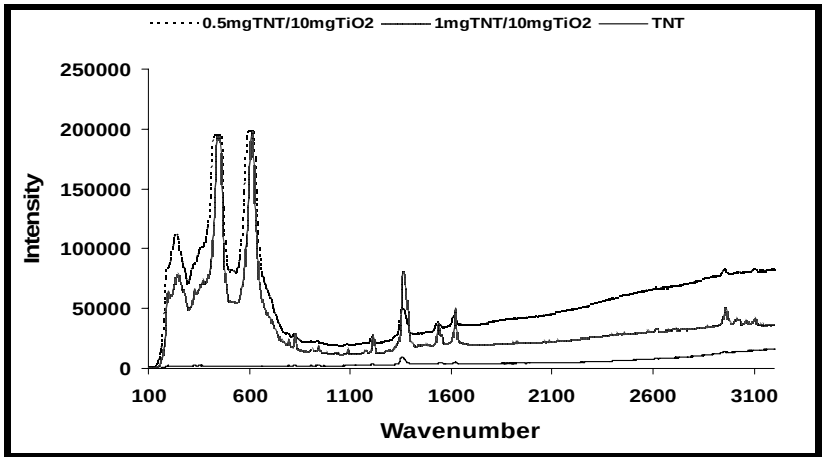

Figure 9: Different proportions of TNT and TiO_2 for different Mixtures of rutile and anatase: low rutile percent.

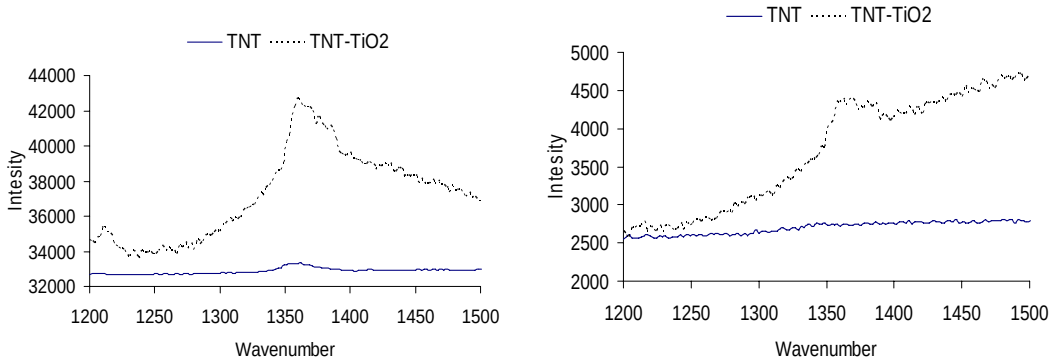

Figure 10: Raman traces TNT and TNT-TiO_2 visible with 100x objective and Raman traces of TNT and TNT-TiO_2 visible with 250 x objectives.

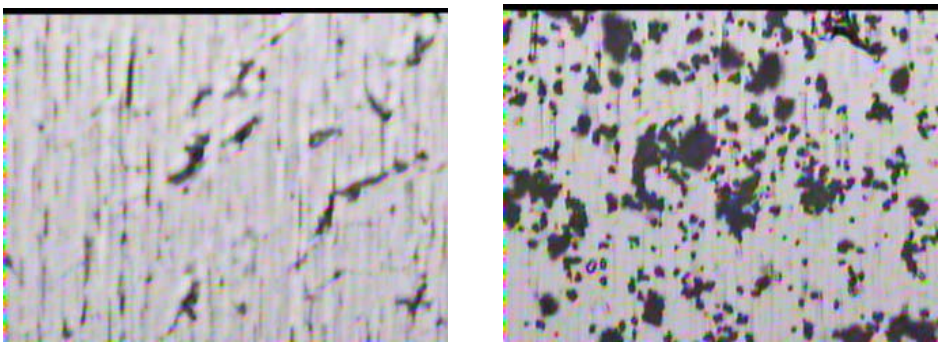

Figure 11: Raman and white light traces of TNT deposited by thermal inject without TiO_2 (left) and with TiO_2 (right).

In Figure 10, the strong increase of TNT signal when it interacts with TiO_2 is observed. Figure 11 shows the micrographs of the experiment.

4.2.2 Raman spectra of TNT on Anatase-Rutile mixtures

The figure12 shows the collection of SERS spectra of TNT obtained with titanium IV oxide mixture different percents of Anatase and Rutile. In all samples was detected TNT in concentrations of $1*10^{-2}$ M except the sample treat with KBr. An increase in the intensity of the signal was observed strongly for the spectrum of greater concentration of Rutile, specific for 1359 c.m-1 characteristic band for nitro groups. In Raman spectroscopy a 10^{-2} M solution is not easily to detect.

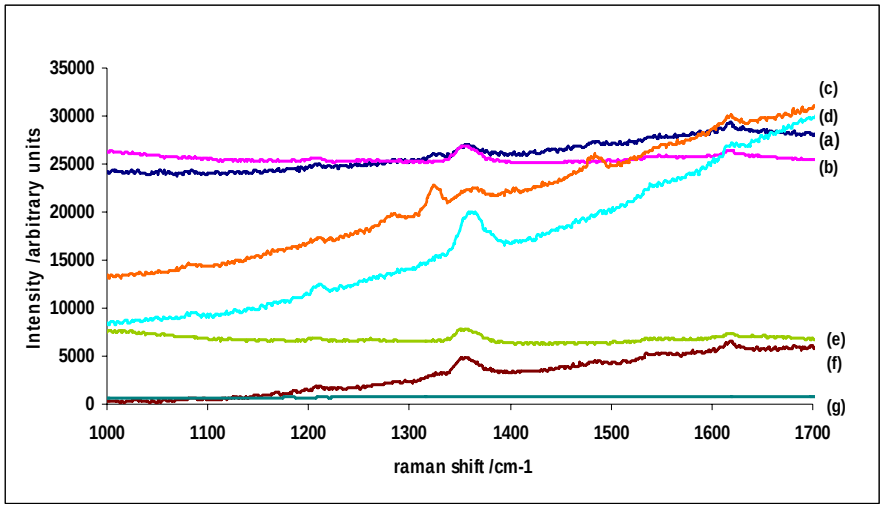

Figure 12: Spectrum of 1.0µL of TNT $1*10^{-2}$ M deposited over tablets of Anatase-Rutile mixture in different proportions (a) 20-80%, (b) 40-60%, (c) 60-40%, (d) 70-30%, (e) 80-20%, (f) 100%, and (g) KBr, respectively.

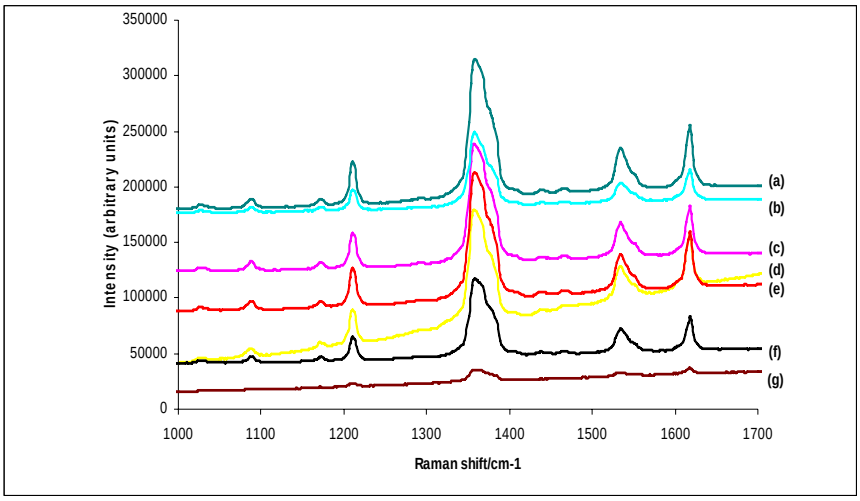

Figure 13: SERS of 1.0mg of TNT mixture Anatase-Rutile in different compositions: (a) 100% rutile, (b) 10-90%, (c) 30-70%, (d) 50-50%, (e) 70-30%, (f) 90-10% respectively and (g) 100% Anatase, and additionally all compared with KBr standard.

The figure 13 shows the collection of spectrum Raman correspond to the NO_2 group; the band at about 1359 cm^{-1} of 1.0mg of TNT added to titanium IV oxide with different ratio of Anatase and Rutile. The spectra composition intensities of 100% Rutile (a) are greater than the 30-70% Anatase-Rutile(c).

Of the table 1 is possible observed that the three intensities with greater increase are those in which the proportion of Rutile is 100, 70 and 50 percent, respectively. Presenting a deviation with respect to the area when increase of the phase Rutile in the mixture 30% Anatase, 70%rutilo

Table 1: TNT 1359 cm^{-1} NO_2 band intensities for different anatase-rutile mixtures.

Composition	Relative Intensity	Increase	Area
100% rutile	120	686	4.19×10^6
10% anatase/90 % rutile	66	377	2.21×10^6
30% anatase/70 % rutile	110	629	3.43×10^6
50% anatase/50 % rutile	104	594	3.84×10^6
70% anatase/30 % rutile	90	514	$\underline{7.70 \times 10^6}$
90% anatase/10 % rutile	69	394	2.77×10^6
100% anatase	9.000	51	2.52×10^6

4.2.3 Raman Spectra of TNT on Nanocrystalline Anatase Titania

Figure 14 shows the XRD patterns of Titania derived from alcoxide hydrolysis precipitation, followed by calcinations for 2h. The samples were synthesized with water/ alcoxide ratios of (a) 3.3, (b) 25 and (c) 100. Anatase nanocrystalline materials were obtained with grain sizes of 38 nm, 24 nm and 7 nm respectively. Figure shows 15 Raman spectra of the nanocrystalline being observed the bands characteristics of anatase. The diminution of the bands that corresponds to sample (a) must to its little crystalline, was followed by hydrothermal to very low temperature with respect to the others.

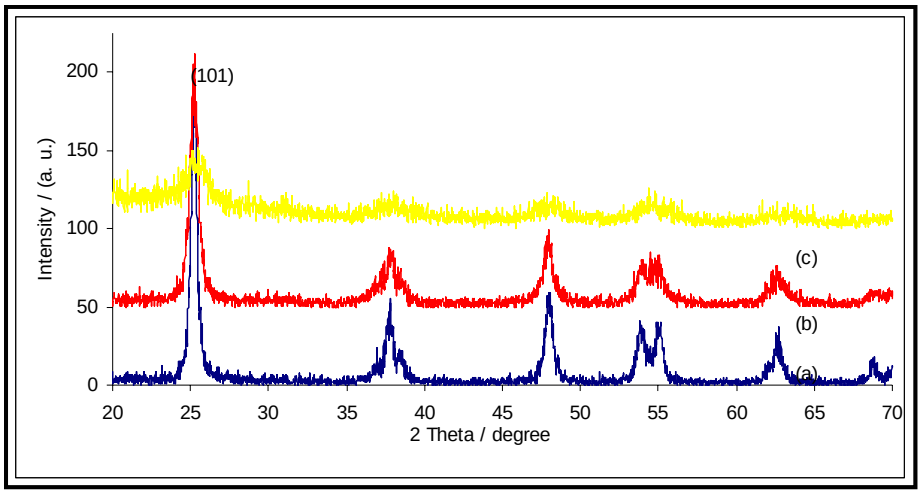

Figure 14:XRD patterns of nanocrystalline Anatase Titania samples prepared with a water: alkoxide ratio of (a) 3.3 (38 nm, without acid), (b) 25 (24 nm, without acid), (c) 100 (7 nm, with HCl acid). The samples were characterized after calcinations at 450 °C for 2h. All peaks noted corresponded to the anatase phase. The crystallite sizes indicated in parentheses were calculated from peak broadening of the anatase (101) diffraction**.**

The amount of acid added or pH of system affects the state of hydrolyzed products in the form of sol-gel and precipitates. The presence of acid catalysis promotes the hydrolysis reactions versus the condensation reaction. HCL serves not only as an acid catalyst, but also as an electrolyte to prevent particle growth or agglomeration through electrostatic repulsion. Since the isoelectric point of TiO_2 lies at a pH of 5-7, surface changes on the particles in an acidic medium help to keep discrete particles in the dispersed state. The SERS spectra of TNT are presented in Figure 16. The increase of the signal is suitable for the decrease in the nanocrystal size as is observed in spectra of trace (c).

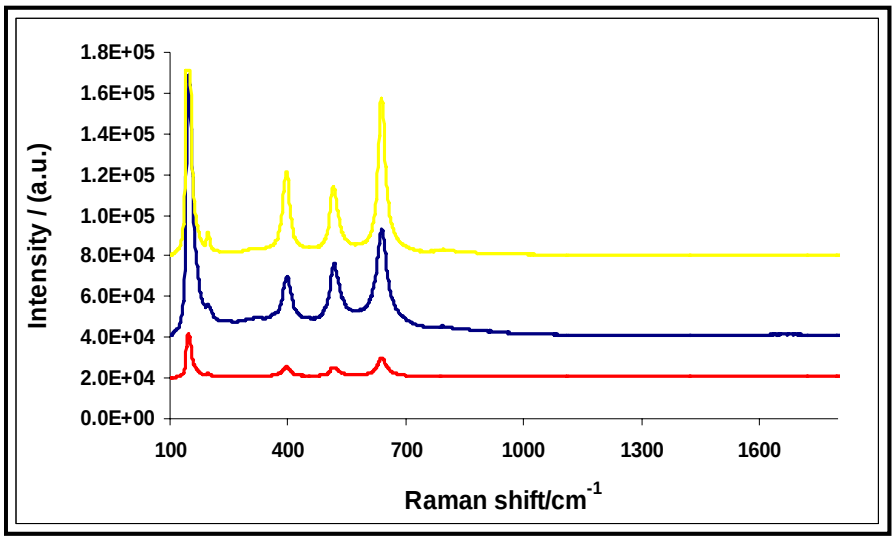

Figure 15: Spectra Raman of nanocrystalline anatase Titania prepared with different size (a) 38 nm (without acid), (b) 24 nm (without acid), (c) 7 nm (with HCl acid).

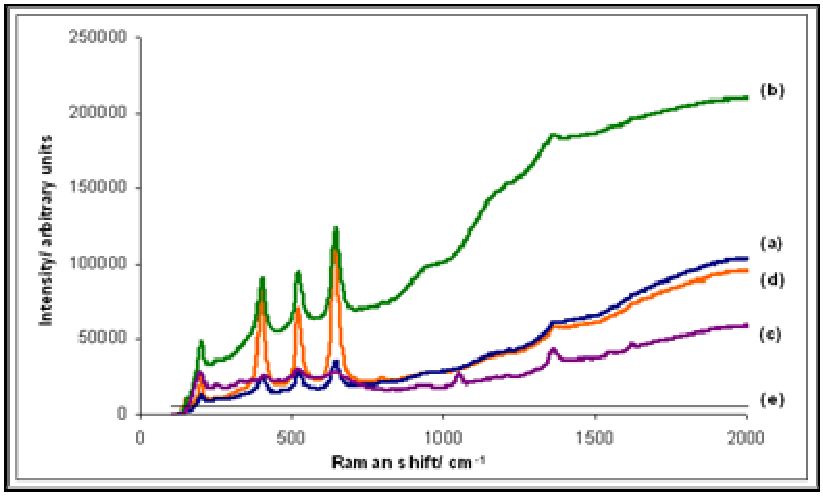

Figure 16: Spectra SERS of nanocrystalline Anatase Titania samples prepared with different size (a) (without acid) (38 nm), (b) (without acid) (24 nm), (c) (with HCl acid) (7 nm), (d) bulk and (e) KBr, mixture with 0.5mg of TNT.

4.2.4 Raman Spectra of TNT on Colloids Suspensions of TiO_2

The results obtained in these experiments could not corroborate the increase found in the previous experiments. The interaction of TNT and titanium dioxide in colloid form did not show a possible effect SERS in anyone of the attempts to increase the signal like: variation of pH, acquisition time, analyte-colloid proportion and particle size. This behavior was

confirmed as much as for nitro group vibration as for all signal that corresponding to trinitrotoluene. These results can be observed in Figures: 17-20.

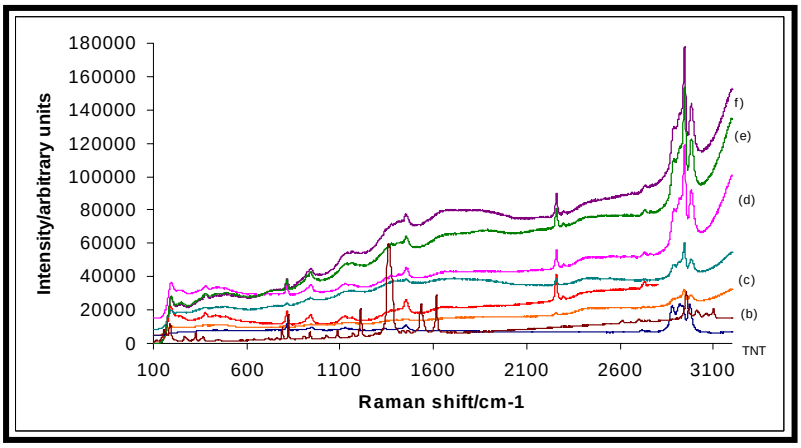

Figure 17: Spectra of TNT with TiO_2 colloid A (25 nm) at different pH: (a) 2.4, (b) 4.2, (c) 7.2, (d) 3.3, (e) 10.9, (f) 12.3. Raman spectrum of neat TNT has been included as reference.

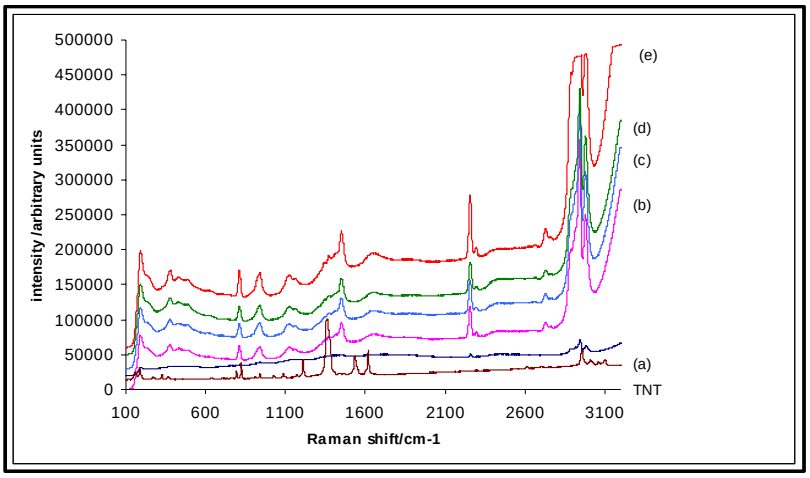

Figure 18: Spectra of TNT with TiO_2 colloid A (15 nm) to pH: 7.24 at different acquisitions time: (a) 10 s, (b) 20 s, (c) 40 s, (d) 60 s, (e) 30 s, and TNT.

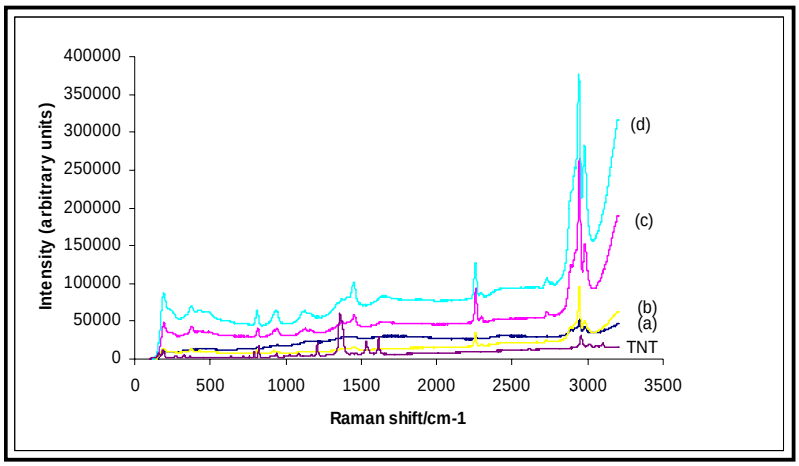

Figure 19: Spectra of TNT of 1*10-3 M with TiO_2 colloid A to pH: 7.24 at different ration TNT: colloid recorded to 60s of acquisition (a) 100µL-800µL, (b) 200µL -600µL, (c) 300 µL-600 µL, (d) 400 µL-600 µL respectively and TNT.

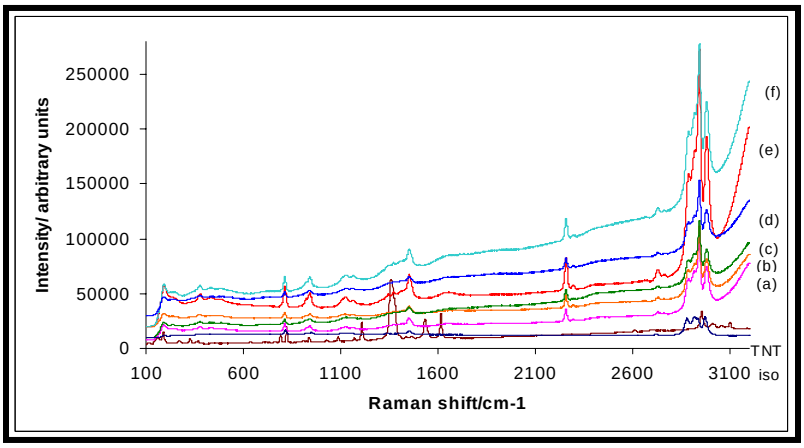

Figure 20: Spectra of 1x10-3 M TNT with TiO_2 colloid B (40 nm) recorded at 10 s at different pH: (a) 2.4, (b) 3.3, (c) 11.0, (d) 12.4, (e) 7.2, (f) 11.8 and TNT.

4.2.5 Raman spectra of TNT on colloids of Ag-TiO_2

The figure 21 shows the UV-VIS absorption spectra of colloidal suspensions of Ag nanoparticles (blue) colloids of Titania (gray) and Titania-coated Ag nanoparticles suspension of Ag (black). The concentration of Ag nanoparticles in the suspension decreased after coverage with TiO_2. The spectrum of the suspension of Ag nanoparticles had a surface plasmon of 420 nm arising from the particles, and the color of the suspension was yellow, in which is characteristic of Ag colloidal dispersion. Similar surface plasmon absorption due to Ag nanoparticles was observed for the suspension of Titania-coated Ag

anoparticles at longer wavelength than for the suspension of Ag nanoparticles. This absorption shift is caused by refractive index of Titania and suggests coverage of Ag nanoparticles with Titania[37].

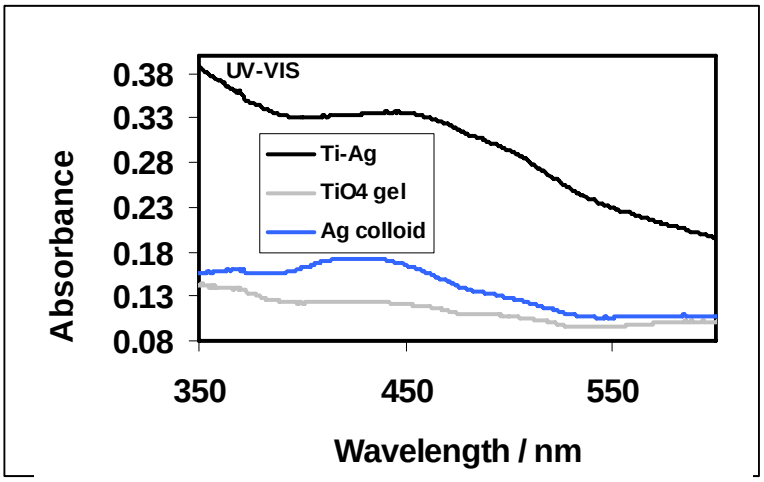

Figure 21:UV-VIS spectra of TiO_2 colloids (bottom) Ag nanoparticles (center), and coated Ag/TiO_2 nanoparticles (top).

The figure 22, exhibits O, Ag, and Ti peaks, showing that the nanoparticles are composed of Ag and TiO_2.

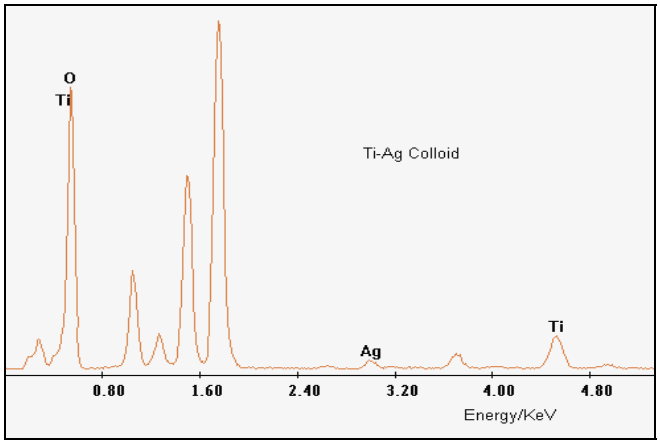

Figure 22: EDAX spectra for Ti-Ag Colloid taken by JEOL 6460LV Scanning Electron Microscope.

Kneipp et al [34] reported SERS from TNT adsorbed on colloidal silver and gold in aqueous suspensions. Spectra were measured down to 10^{-7} M TNT. They observed clear, strong bands in the spectrum at about 1000 cm^{-1} (ring breathing mode). This vibration is very

weak in the normal spectrum of TNT. The bands at 1359 and 1204 cm^{-1} were slightly shifted to higher wavenumbers. Figure 23 shows the SERS spectrum of solution of $1x10^{-3}$ M TNT at different pH with Ag–TiO_2 coated colloidal suspensions. At pH = 10.3 the SERS spectra showed an increase of the NO_2 stretching mode at the 1365 cm^{-1} in comparison with the other pH values and the solution of $1x10^{-3}$ M without colloids. Additionally, the band 1213 cm^{-1} and NO_2 band are shifted to higher wavenumbers.

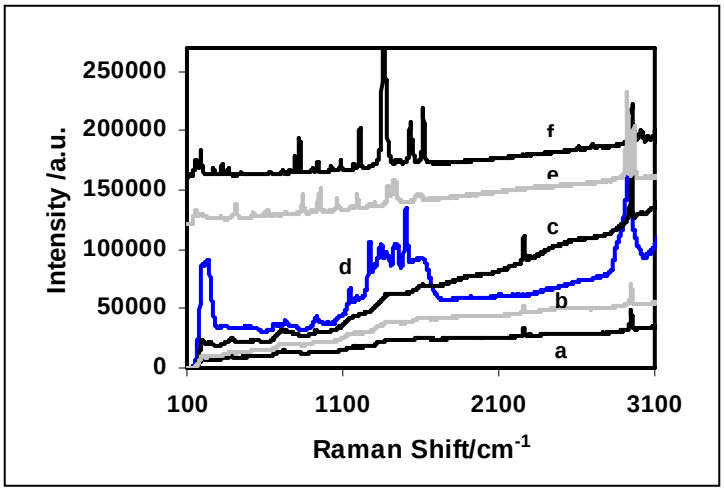

Figure 23: SERS spectra recorder with laser 532nm of TNT with Ag -Ti colloid at different pH: a. 12.3; b. 13.5; c. 10.3; d. 11.3; e. citrate and f. neat TNT.

Figure 24 shows a series of SERS spectra recorded at 532 nm excitation wavelength of TNT at different concentration: a. $1x10^{-3}$M, b. $1x10^{-4}$ M, c. $1x10^{-6}$M and d. $1x10^{-8}$M obtained at pH = 10.3. Results show an increase of NO_2 stretching mode in the range of 1300-1370 cm^{-1} down to a concentration of $1x10^{-6}$M, although this vibration has very low intensity. Figure 25 shows SERS spectrum of solution of $1x10^{-3}$ M TNT to different pHs with Ag-TiO_2 colloid. The aromatic ring breathing mode was observed near 1000 cm^{-1} which was not observed in spectrum acquired at 532 nm. Also, the bands observed for TNT were the asymmetric stretching 1555-1587 cm^{-1} NO_2 and symmetric NO_2 stretch at 1300-1357cm^{-1}. This was found especially to pH 10.3 and at acid pH ~ 6.5. This vibrations where observed even at smaller concentrations that the ones in the realized experiment with the laser of 532 nm. This is illustrated in Figure 26 where the bands are detected as low as $1x10^{-10}$ M TNT when 488 nm is used as excitation source.

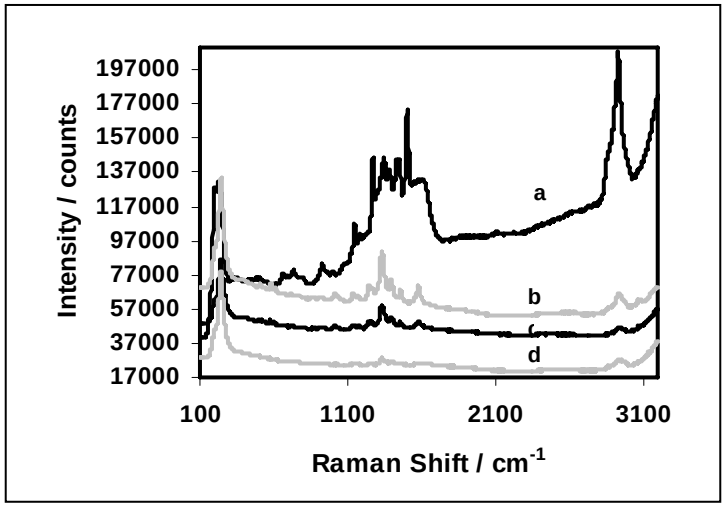

Figure 24: SERS spectra recorder with laser 532nm of TNT to different concentration: a-$1*10^{-3}$M, b- $1*10^{-4}$ M, c-$1*10^{-6}$M and d-$1*10^{-8}$M obtained with same pH 10.30

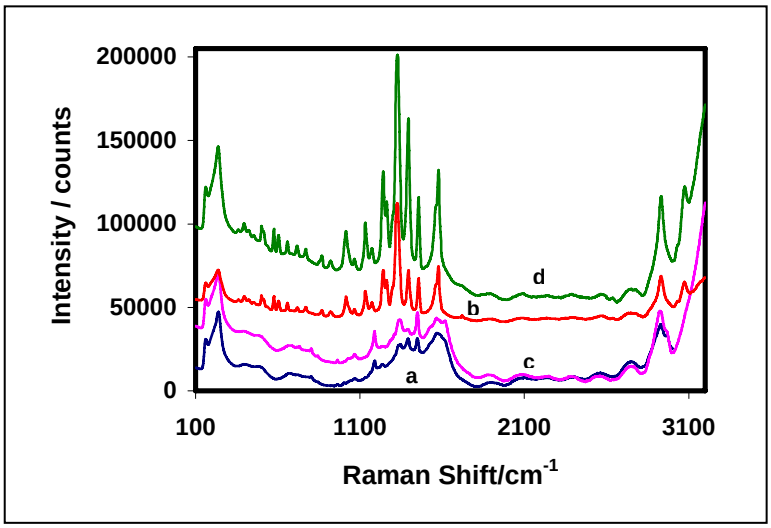

Figure 25: SERS spectra recorder with laser 488nm of TNT with Ag –Ti colloid at different pH: a 13.30, b 12.60. c 6.50, d 10.40, e citrate, and f TNT.

Figure 27 shows SERS spectra of $1x10^{-3}$ TNT M solutions recorded with portable Raman spectrometer operating at 785 nm at different pH with Ag-TiO_2 colloid. In addition, of observing in this spectrum, the symmetric and asymmetric vibration modes corresponding to the nitro and aromatic ring group of the TNT, it is also seen vibrations in the region included between 150-700 cm^{-1} that are not solved in the obtained spectrum with the two

anterior wavelength. The spectrum with the best resolution where obtained with a pH 10.6 and slightly acid 6.2 being this the same with 488 nm as wavelength.

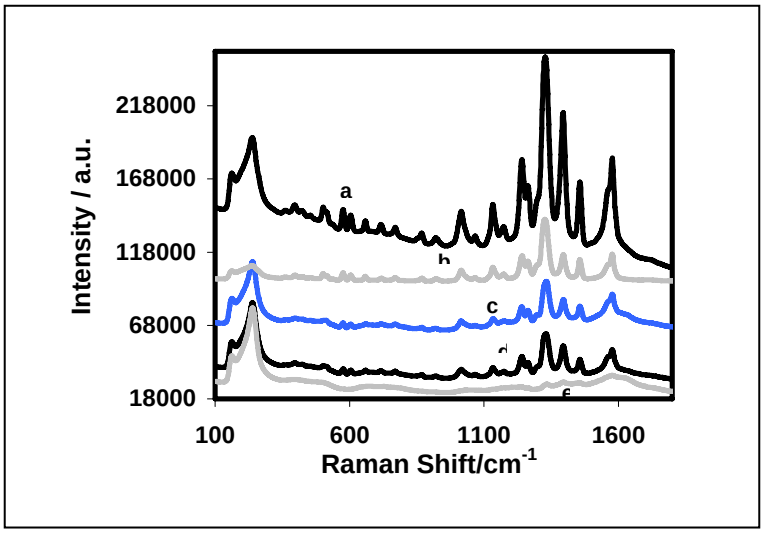

Figure 26: SERS spectra of TNT recorded at 488 nm excitation with Ag –Ti colloid for different concentrations: a. $1x10^{-3}$M, b. $1x10^{-6}$ M, c. $1x10^{-8}$ M, d. $1x10^{-10}$ and e. $1x10^{-12}$M.

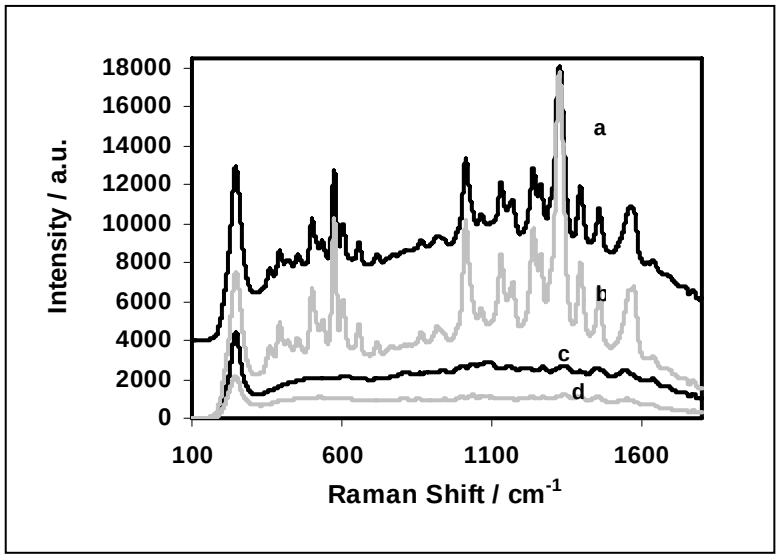

Figure 27: SERS spectra recorded with portable Raman spectrometer at 785nm of TNT solutions with Ag –Ti colloid at pH: a. 6.2, b. 10.6. c. 12.4 and d. 13.1.

For the experiments carried out at 785 nm, very good definition and intensity enhancements of vibrational signals were observed down to $1x10^{-8}$M as can be observed in Figure 28.

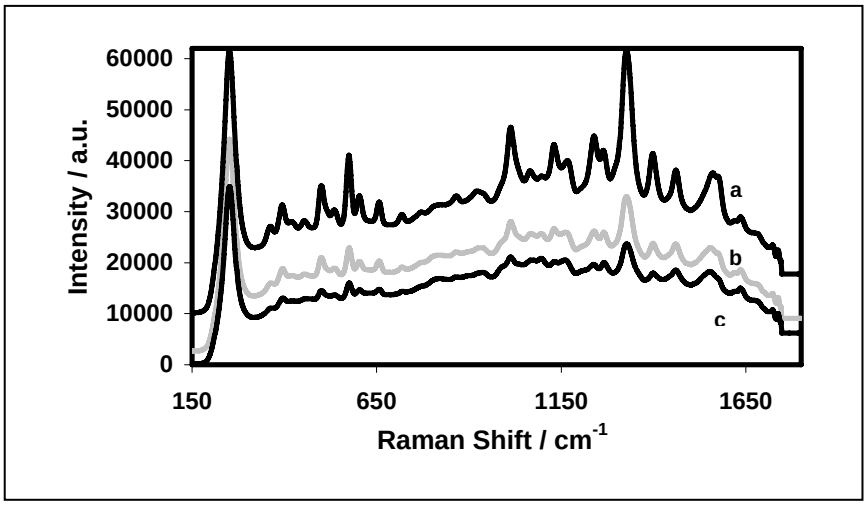

Figure 28: SERS spectra of TNT recorded with portable 785 nm with Ag –Ti colloid at pH 10.6 different concentration: a. $1x10^{-3}$M, b. $1x10^{-6}$ M, and c. $1x10^{-8}$ M of TNT.

SERS spectra of TNT with portable Raman spectrometer 532 nm excitation manufactured by Raman Systems, Inc. are presented in Figure 29, in which the increase of the Raman signals were observed in a $1x10^{-6}$M TNT solution. There is not much difference in the vibrational modes found with respect to the observed in the spectrum obtained to this same wavelength but with a non-portable Raman system.

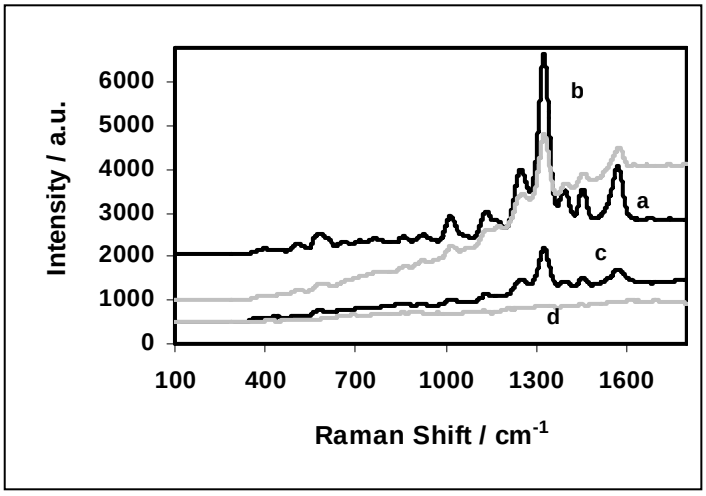

Figure 29: SERS spectra of TNT recorded with portable Raman spectrometer of 532 nm excitation with Ag –Ti colloid at pH 10.4 for: a. $1x10^{-3}$M, b. $1x10^{-4}$ M, c. $1x10^{-8}$ M and d. $1x10^{-8}$ M.

Chapter V

Photodegradation Kinetics of Nitroexplosives

5.1 METHODOLOGY

5.1.1 Reagents and instruments

The crystalline samples of TNT and 2,4- and 2,6-DNT used for the experiments described here were purchased from Chem Service Inc., West Chester, PA (crystals, 98%, 30% water). Titanium (IV) oxide nanocrystals were derived via sol-gel hydrolysis precipitation of titanium isopropoxide (Ti $(OC_3H_7)_4$) (Alfa Chemical Co., MA). The concentrations of the organic compounds were monitored with a high performance liquid chromatograph equipped with a UV detector. The measurements were conducted by measuring the UV absorption at 254 nm. A reverse-phase column, 25 cm long and 4.6 mm in the inside diameter, packed with ODS Hypersil 5μm, a 30°C temperature, isocratic mobile phase, stream of 0.75 mL/min, λ = 254 nm and a 10 μL injection.

5.1.1.1 Measurements

Several experiments were carried out to observe the photocatalytic transformation and kinetics of TNT with anatase Titania nanocrystals. These experiments were made in darkroom, with continuous stirring and bubbling of oxygen.

5.1.3 Control assays

Photochemical control experiments were performed to determine the stability to UV radiation and to verify that the degradation was solely from the photocatalytic source.

a) In the first set of control experiments the solutions were illuminated with UV light at 236 nm, stirring and bubbling oxygen but without TiO_2 nanocrystals.
b) In the second set of control experiments TiO_2 was added to the solutions containing everything else were added and stirring and bubbling oxygen but without illuminating with the UV light source.

5.1.4 Effect of amount of TiO_2

These experiments were performed changing the amount of TiO_2, from 20 to 40, 60 and 80 mg for 50 mL of 4 ppm solution of TNT. These were done to decide the lowest amount of titanium dioxide capable to degrading the organic compounds.

5.1.5 Different concentrations of TNT

The photochemical experiments were performed using 60 mL of solutions of different concentrations of TNT, 2,4-DNT and 2,6-DNT and adding 20 mg of TiO_2. Each suspension stayed in continuous agitation under an oxygen flow. Then, aliquots of 5 mL of different samples at intervals of 20 minutes during 4 hours were taken and filtered with a Millipore membrane of 0.45 μm before carrying out the chromatographic analysis. The concentrations of the organic compounds were monitored with a high performance liquid chromatograph (HPLC), equipped with a UV detector.

5.2 RESULTS AND DISCUSSION

5.2.1 Synthesis of Anatase Nanocrystals

The figure 30 shows the XRD patterns of Titania derived from alcoxide hydrolysis precipitation, followed by hydrothermal treatment during 8h. The samples were synthesized with a water:alcoxide ratio of 100. Anatase nanocrystalline materials were obtained with grain sizes of 20 nm.

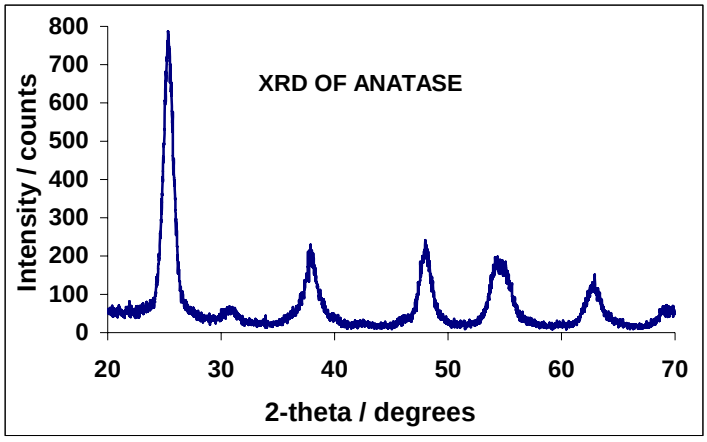

Figure 30: XRD patterns of anatase Titania nanocrystalline samples prepared with water: alkoxide ratio of 100. All peaks noted corresponded to the anatase phase. The crystallite sizes indicated in parentheses were calculated from peak broadening of the anatase (101) diffraction.

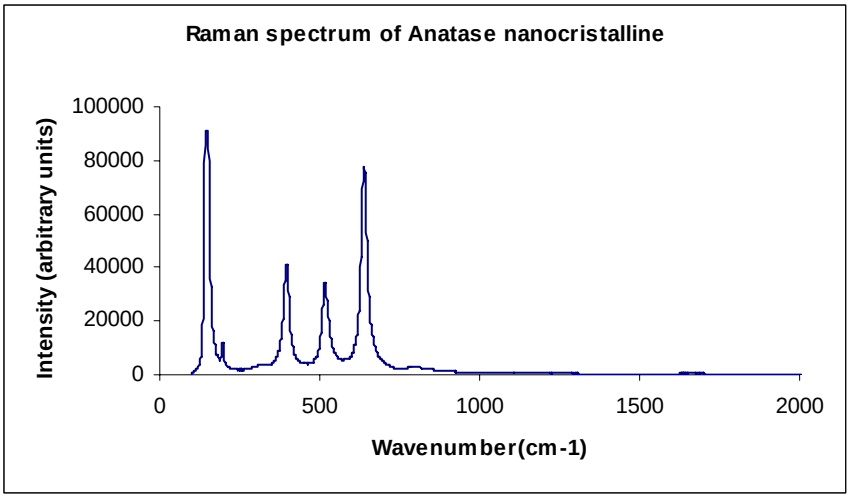

Figure 31: Raman Spectrum of anatase Titania nanocrystalline prepared with hydrothermal treatment to 20 nm of size

5.2.2 10: Control assays

The results obtained from both experiments show that the concentration of TNT (4ppm) doesn't change under these processes separately.

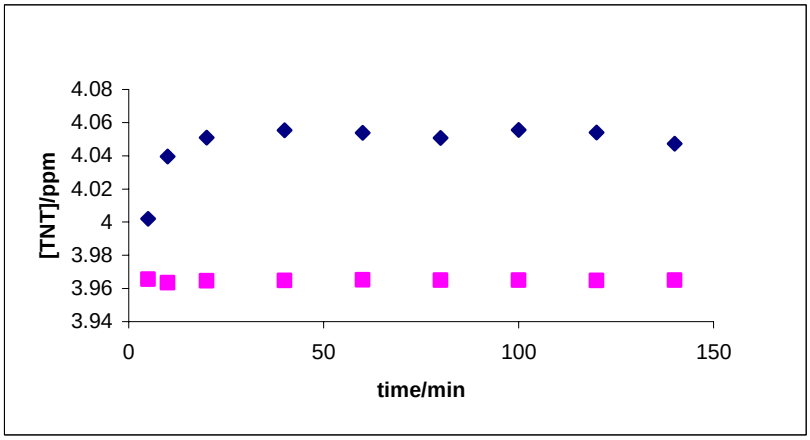

Figure 32: Change in the concentration of TNT during the experiment: ♦ TiO_2 without UV radiation and▪ UV radiation without TiO_2.

5.2.3 Effect of amount of TiO_2

Figure 33 shows the decrease in concentration of 4 ppm solutions of TNT under UV radiation, using different amounts of TiO_2. The curves presented a similar shape to each

other, which indicates that the degradation kinetics should be the same. Increasing the Titania respect to the solution (20-40 mg) increases the photocatalytic degradation of TNT. However, for the interval of (60-80 mg) increase in the photocatalytic degradation action is not observed, demonstrating that the best amount of catalytic is 20 mg, in which permits the photodegradation without any excess of Titania. Figure 34 shows the photocalytic degradation profiles of TNT at different concentrations 3, 5, 8 and 10 ppm with 20 mg of catalytic TiO_2.

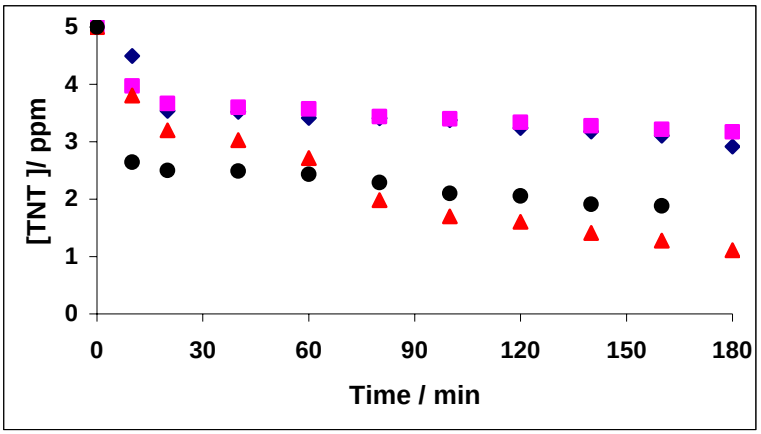

Figure 33: Change in the concentration of TNT during irradiation in aqueous solutions to different amounts of Titania: ▲ 20 mg, ● 40 mg, ♦ 60 mg, ▪ 80 mg.

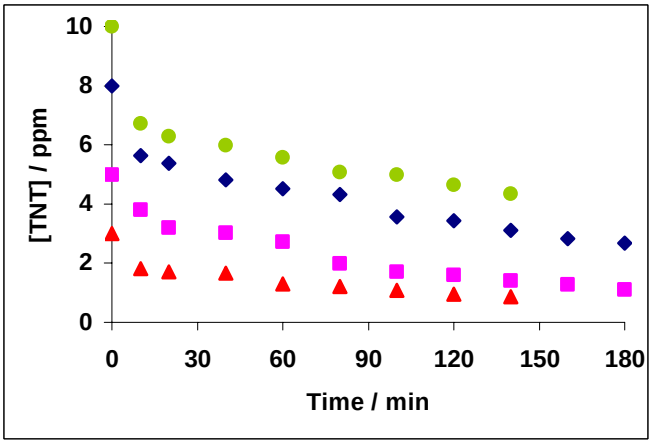

Figure 34: Change in the photodegradation for TNT to different concentrations: ▲ 3ppm, ▪ 5ppm, ♦ 8ppm and ● 10ppm with 20mg of TiO_2.

The results reported above confirm that TNT can be degraded in illuminated TiO_2 suspensions. Recently, it has been proposed that TNT is degraded in irradiated TiO_2

suspensions following two competitive pathways.[38] On the one hand, the methyl group is oxidized in subsequent steps to a carboxyl group. TNB is then formed by decarboxylation of the intermediate benzoic acid. The intermediary formation of TNB in the photocatalytic degradation of TNT can therefore be explained by a side-chain attack of photo generated hydroxyl radicals or by hole oxidation:

$$TNT + h_{vb}^{+} \longrightarrow TNT^{\bullet +} \longrightarrow TNT^{\bullet} + H^{+}$$

$$TNT + {}^{\bullet}OH \longrightarrow TNT^{\bullet} + H_20$$

On the other hand, the degradation can be started reductively by an electron transfer from excited TiO_2 to TNT[39]:

$$TNT + e_{cb}^{-} \longrightarrow TNT^{\bullet -}$$

All the experiments of photocatalytic degradation of Nitroexplosives were carried out at ambient temperature, under of excess of oxygen. The reactions of photocatalytic degradation are companied an important adsorption effect on the semiconductor surface.

5.2.4.1 Kinetic model: **Langmuir-Hinshelwood Model**

According to the results, the expression of photooxidation kinetics of organic solutes can be described by:

$$\mathbf{v = -dC/dt = k\ KC/1+KC}$$

Then,

$$\mathbf{1/v = 1/k\ KC + KC/k\ KC}$$

And then reduced to

$$\mathbf{1/v = 1/k + [1/kK]\ 1/C}$$

In which, if the method is correct, the data is plotted 1/v as function of 1/C and obtain the straight-line relationship with intercept 1/k and slope 1/k-K. In this way, it could be calculated the parameters ***k***, the reaction rate constant and **K**, the adsorption equilibrium constant. The initial rates were calculated considering the first ten minutes of reaction by means of the expression:

$$\mathbf{v = [mol/\ L.\ min] = -\ \Delta\ concentration\ [mol/L]\ /\ \Delta\ time\ [min]}$$

The reciprocal values of initial rates of the photodegradation reactions were tabulated versus the reciprocal values of the initial concentrations and then were plotted[40].

Table 2: Initial rates of TNT photooxidation reaction.

Concentration [ppm]	**1/Concentration initial $[mg/L]^{-1}$**	**1/v rate initial $[mg/L.min]^{-1}$**
9.96±0.07	0.10	3.05±0.07
7.98±0.1	0.13	4.2±0.2
4.8±0.2	0.20	8.33±1.71
3.03±0.07	0.33	12.04±0.8

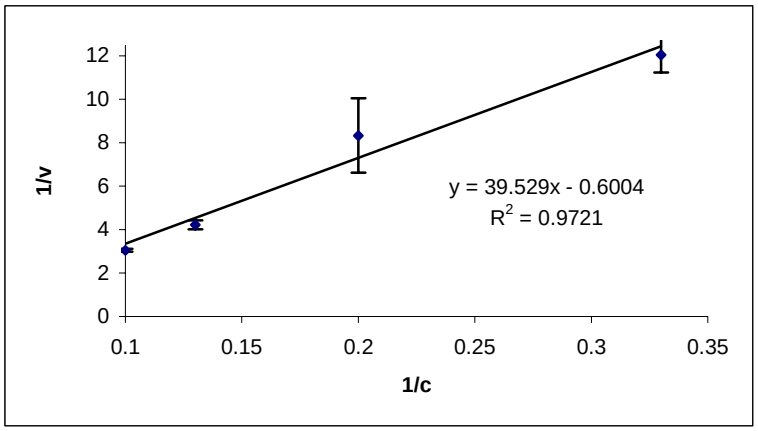

Figure 35: Reciprocal of initial reaction rate v/s reciprocal initial concentration of TNT.

Based on Figure 35, the straight-line relationship of reciprocal of initial reaction rate v/s reciprocal initial TNT concentration, confirms the validation of Langmuir-Hinshelwood model and that the photooxidation reactions occur completely in the titanium dioxide surface.

In this case, the straight-line is obtain with intercept 1/k = 0.6004, means a reaction rate constant of ***k* = 1.67 [mg/L.min]** and a slope 1/k K = 39.529, and means an equilibrium adsorption constant **K= 1.5 * 10^{-2} [L/mg].** These results are consistent with the found ones by Kyung Duk et al.[41], who found values of ***k* = 1.78 [mg/L.min]** and **K = 0.093 [L/mg]**. The photodegradation process of 2,4- and 2,6-DNT also was analyzed with the Langmuir-

Hinshelwood Model due to its linear behavior, plotting reciprocal initial rate versus reciprocal concentration, such as is observed in Figures 36-37.

Table 3: Initial rates of 2,4-DNT photooxidation reaction

Concentration [ppm]	1/Concentration initial $[mg/L]^{-1}$	1/v rate initial $[mg/L.min]^{-1}$
15.99±0.02	0.06	10.8±1.2
11.97±0.01	0.08	14±2
9.99±0.02	0.1	14.8±0.4
7.98±0.05	0.12	20±5
2.95±0.03	0.33	27.7±2.28
1.97±0,09	0.55	36.2±0.2

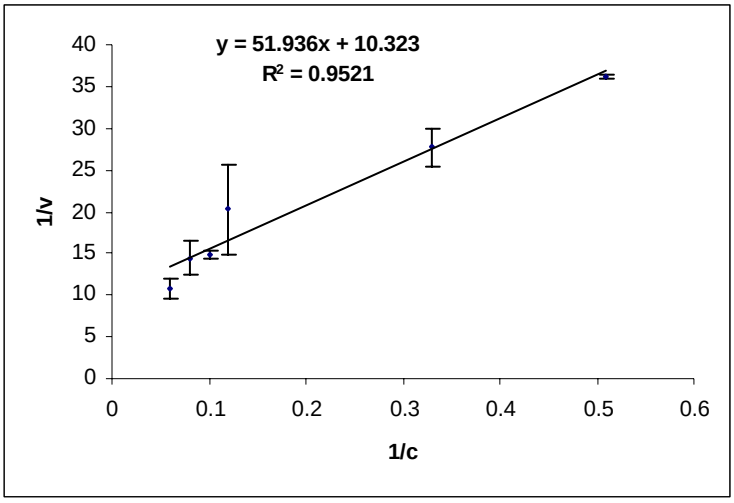

Figure 36: Reciprocal of initial reaction rate vs. reciprocal initial concentration of 2,4-DNT

Table 4:. Initial rates of photooxidation reaction of 2,6-DNT

Concentration [ppm]	1/Concentration initial $[mg/L]^{-1}$	1/v rate initial $[mg/L.min]^{-1}$
15.98±0.08	0.06	2.98±0.07
12.07±0.11	0.08	3.55±0.13
9.98±0.02	0.1	3.73±0.04
7.98±0.23	0.12	5.6±0.8
5.12±0.04	0.19	15.62±0.93
3.12±0.02	0.33	22.70±1.04
1.96±0.01	0.55	52.7±5

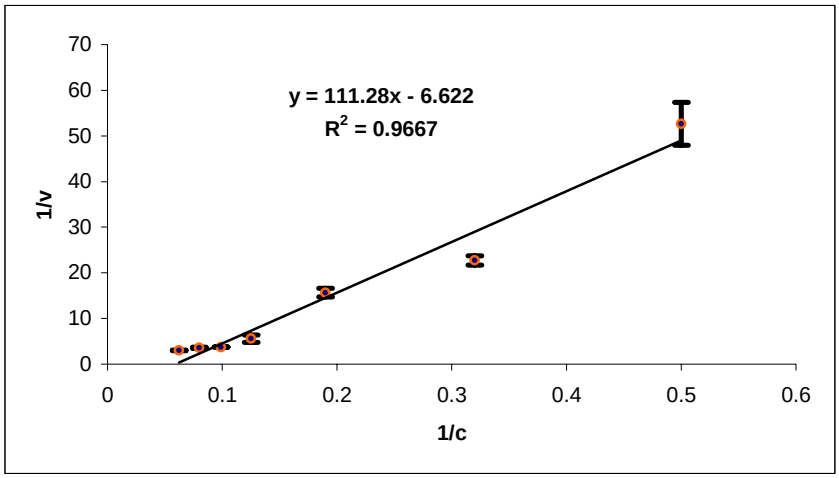

Figure 37: Reciprocal of initial reaction rate vs. reciprocal initial concentration of 2,6-DNT

In the case of 2,4-DNT a reaction rate constant of k = 0.096 [mg/L.min] was obtained and an equilibrium adsorption constant K = 2.0×10^{-1} [L/mg]. For 2,6-DNT constant of reaction rate k = 0.12 [mg/L.min] was obtained with an equilibrium adsorption constant of K = 5.9×10^{-2} [L/mg]. According to the numerical results there is a difference of an order of magnitude with respect to both equilibrium adsorption constants. This result is possibly due to nitro group position in the structure of ring if is presumed that the adsorption of explosive on semiconductor take place via the nitro group. The calibration curves used for the calculation of different explosives are in the appendix A.

Chapter VI
CONCLUSIONS

The results presented here clearly demonstrate that the vibrational signals of the Raman spectra of the target nitroaromatic explosive TNT is strongly enhanced by the presence of the TiO_2 surface. The studies indicate that the anatase crystal size influences the magnitude of the Raman signal enhancement of 0.5 mg of TNT, which is observed, in particular for the sample with average crystals size of 7 nm. Since Raman signal enhancement is evident in these experiments, other mechanisms could be responsible for the enhancement factors, because a large signal enhancement was not found when the target explosive was interacted with TiO_2 colloids.

In summary, Ag–TiO_2 covered colloids were prepared where silver colloid absorption maximum shifts to longer wavelengths, which could provide a proof of the interaction of metal and semiconductor. This study indicates that the Ag–TiO_2 colloid is also useful as a powerful tool for SERS. The result also demonstrates that Raman signals of the target nitroaromatic explosives TNT are strongly enhanced by colloid at the different excitation wavelengths: 488, 785 and 532 nm. This is observed especially for the SERS spectrum of solution $1x10^{-8}$ M TNT at pH 10.4 recorded with 488 nm laser. The aromatic ring breathing mode was observed near 1000 cm^{-1}, to asymmetric stretching was located at 1555-1587 cm^{-1} NO_2 and the symmetric NO_2 was located at 1300-1357cm^{-1}

The combined action of TiO_2 and UV light induce the efficient photocatalytic destruction of organic compounds, such as TNT and DNT, which are polluting agents. The decrease percentage in TNT and DNT concentration, resulting from the photocatalytic reactions conducted for 140 min, were 70% and 75%, respectively. TNT and DNT degradation followed a pseudo first order rate expression according to the Langmuir-Hinshelwood kinetic model.

REFERENCES

1. Baker, J., Richard Colton, Schroeder-Gibson, H., Grunze, M., Lee, S., Klabunde, K., Martin, C., Murday, J., Thundat, T., Tatarchuk, B., and Ward, K., Grand Challenge Workshop Series, November **2002**, Monterrey, California.
2. Mercado, L, Torres, Gomez, L., Mina, N., Hernández, S.P., Chamberlain, R.T., Lareau, R. and Castro, M.E., *J. Chem. Phys. B*, **2004**, vol 108, pp 12314-12317.
3. Cooper, P., Kuruwski, R. S. *Introduction to the Technology of Explosives.* **1997**.
4. Garg, R., Grasso, D., and Hoag, G. *Hazardous waste and Hazardous Mat **1991**, 48*, 319.
5. Spiker, J. K., Crawford, D. L., and Crawford, R. L. *Appl. Euviron. Microbial, **1992**,* 3199.
6. Michels, J. and Gottschalk, G. *Appl. Environ. Microbial. IB(T,* **1994,** pp *187.*
7. Akhavan, J. *The Chemistry of Explosives*, 1st ed.; The Royal Society of Chemistry: Massachusetts, **1998**; pp 45-60.
8. Ferraro**,** J.R., Nakamoto, K. *Introductory Raman Spectroscopy*. Academic Press, California, **1994**, pp 13-26.
9. Clarke, R.H., Londhe, S., Premasiri, W.R. and Womble, M.E., *J. Raman Spectrosc*. **1999**, 30, pp 827–832.
10. McCreery, R.L. *Raman Spectroscopy for Chemical Analysis*. John Wiley & Sons, New York, **2000,** pp 326-327
11. Buttner, M.; Findlay, W.; Davis, M. *Analytical Chemical Acta* **1997**, pp 63-71.
12. George V., Jenkins, T.F., Leggart, D.C. and Cragin, J.H., *Proceedings of SPIE* 3710, 258, SPIE. Bellingham, WA, **1999**.
13. Perez, R. *Procesado y Optimizacion de Espectros Raman Mediante Tecnicas de Logica Difusa: Aplicacion a la Identificacion de Materiales Pictoricos.* Department of Teoria del Senyal I Comincacions, Submitted in partial fulfillment of the requirements for the degree of Doctor of Philosophy Chemistry. **2005**, Cataluña: España.
14. Shimbamoto, K., Katayama, K., Fujinami, M. and Sawada, T., *Analytical Science.* **2001**, vol 17. pp, 191-194.

15. Morishita, T., Hibara, A., Sawada, T., Tsuyumoto, I. and Heart, A., *Anal. Sci.,* **2000**, vol *16*, pp 403.

16. Peiro, A. *Nuevas Aportaciones al Desarrollo de Metodologías en Química Verde: Eliminación Fotocatalítica de Contaminante Fenólicos, Preparación de Fotocatalizadores Mediante Procesos Químicos Suaves*. Department of Chemistry, Submitted in partial fulfillment of the requirements for the degree of Doctor of Philosophy Chemistry. **2003**, Bellaterra: España.

17. Parra, S., Olivero, J., Pacheco, L., Pulgarin C., *Applied Catalysis B: Environmental.* **2003**, vol *43*, pp 293–301.

18. Jing, S., Xie, Q., Shuo, C., Ya-shi, Z. and Guo-Hua, C., *Journal of Enviromental Sciences*. **2003**, Vol *15*, No 1, pp 60 –64.

19 Hong Park, J., Choi, E. and Gil, K., Journal *of Enviromental science and health.* **2003**, Vol A*38*, No 7, pp 1389 – 1399.

20. O'Neil, C. *Chem. Technol. Biotechnol.* **1999,** vol *74*, pp 1009.

21. Sankar, M. *Chem. Technol. Biotechnol.* **1999,** vol *74*, pp 337.

22. Paggan, N. and Brown, D. Chemosphere, **1986**, vol *15*, pp 479.

23. Medina-Valtierra, J., Garcia-Servin, J., Frausto-Reyes, C and Calixto, S., *Mexican Journal of Chemical Engineer* **2005,** vol 4, pp 191-201.

24. Hyun-Seok, S., Son-Jin, L., Hyoung, C. and Kyung-Duk, Z., *Chemosphere.* 2004, vol 57, pp 309-317.

25. Arenas, J., Pelaez, F. D., Lopez Ramirez, M.R, Castro, J.L. and Otero, J.S., *Opt. Pur and Appl*. **2004,** Vol. *37*, Num. 2**,** pp 637-642.

26. Hui-Hua, D., Whang, X., Tsing, Y., Hai-fang, M., Toshishige, S. and Zu-Hong, L., *Chinese Physics*. **2001**. Vol *316*, pp 3113-3120.

27. Millis, A. and Valenzuela, M.A., *Rev. Mex. Fis*. **2004.** pp 287.

28. Chen-Chi, W.; Jackie, Y .*Chem. Mater*. , **1999,** vol 11, pp 3113-3120.

29. Linsebigler, A. L., Lu, G. and Yates, J.T. *Chem. Rev*. **1995,** vol *95,* pp 735-758.

30. Sylvia, J.M., Janni, J.A. Klein, J.D. and Spencer, K.M., *Anal. Chem*. **2000**, vol 72, pp 5834-5840.

31. Moskovits, M. *Reviews of Modern Physics.* **1985**, vol *57***,** pp 783-826.

32. Lee, P.C. and Meisel, T.J.J. *Phys Chem.* **1982,** vol *86*, pp 3391-3395.

33. Kneipp, K., Wang, Y.., Kneipp, H., Perelman, L.T., Itzkan, I., Dasari, R.R., and Field, M.S. *Phys.l Rev.* **1997,** *lett,* vol *78*: 1667-1669.
34. Keipp, K. *Spectrochim, Acta part A.* **1995,** *vol 51,* pp 2171-2175.
35. W. J. Li, E. W. Shi, and T. Fukuda, *Cryst. Res. Technol*. **2003,** 38, vol. 1, pp, 847-858,
36. Aroca, R.F., Clavijo, R.E., Halls, M.D. and Schlegel, H.B., *J. Phys. Chem. A*. **2000**, vol 104, pp 9500-9505.
37. Sakai, H., Kanda, T., Shibata, H., Ohkubo, T. and Abe, M. *Journal Am. Chem. Soc*. **2006,** pp 1-9
38. Dillert, R., Fornefett, I., Siebers, U. and Bahnemann, D. *Journal of Photochemistry and Photobiology A: Chemistry.* **1994,** vol 94. pp 231-236.
39. Son, H.S., Lee, S. J., Cho, H. I. and Zoh, D. K. *Chemosphere.* **2004***,* vol 57, pp 309-317.
40. Caneo. C., Aedo, G. and Ollino, M. *XII Environmental Engineer Congress.* **1999,** pp 110.
41. Hess, T., Lewis, T., Crawford, R., Katamneni, S., Wells, J. and Watts R. *Water Res*. **1998**, vol 32, pp 1481-1491.

APPENDIX A1

TNT Concentration (ppm)	Average Area
1	53.2 ± 0.3
5	266.2 ± 0.7
10	527 ± 30
25	1329 ± 20

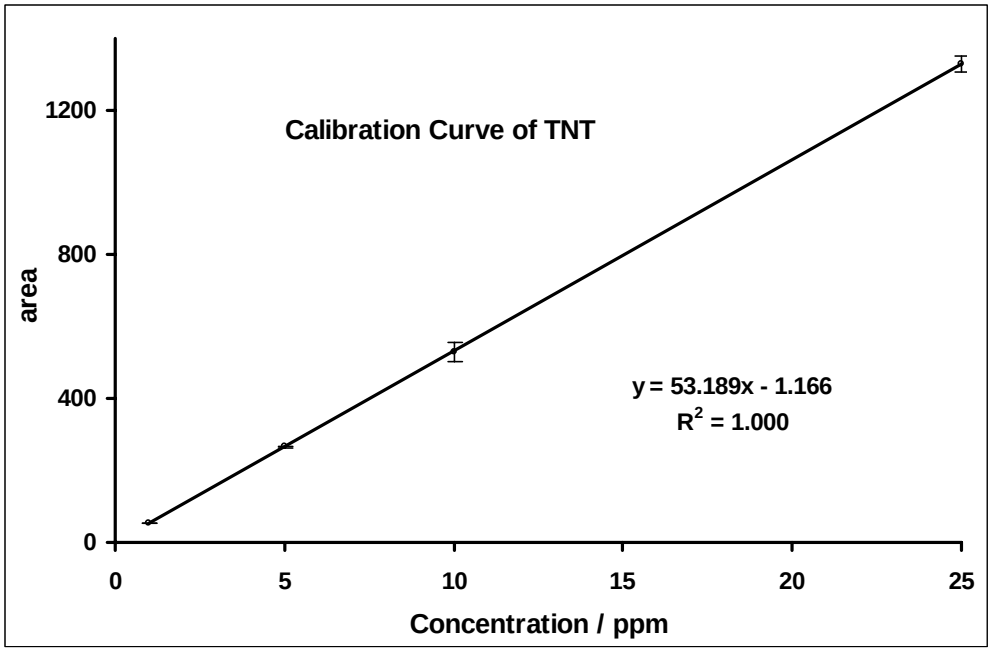

Figure A1: Calibration curve of TNT

APPENDIX A2

Concentration ppm of 2,4-DNT	Area Average
1	61.0±0.1
2	121.2±0.5
5	301.3±0.4
8	471.3±0.2
16	947.0±0.6

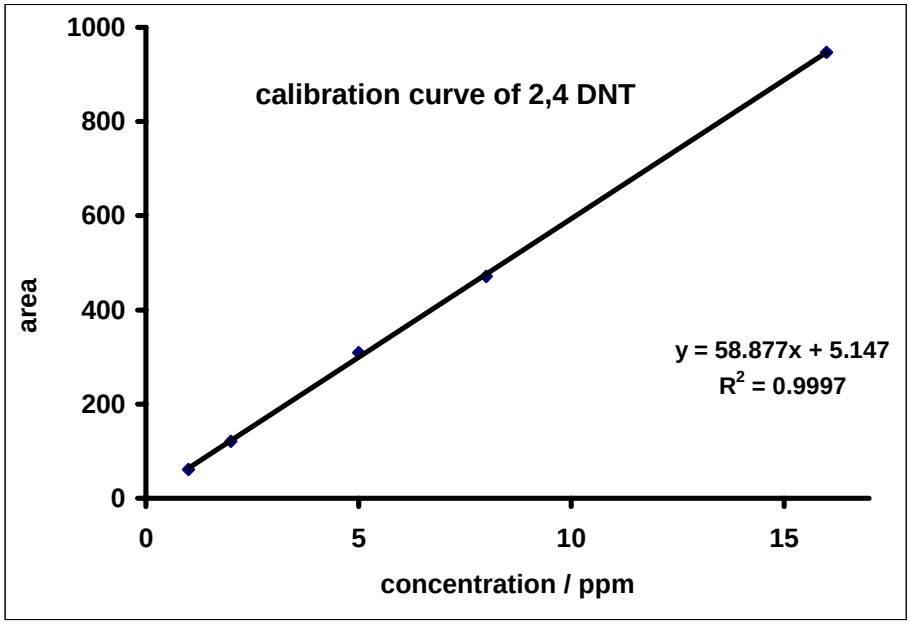

Figure A2: Calibration curve of 2, 4-DNT

APPENDIX A3

2,6-DNT Concentration (ppm)	Average Area
1	32.0±0.1
2	63.5±0.3
5	163.5±0.6
8	261.1±0.2
16	525.5±0.4

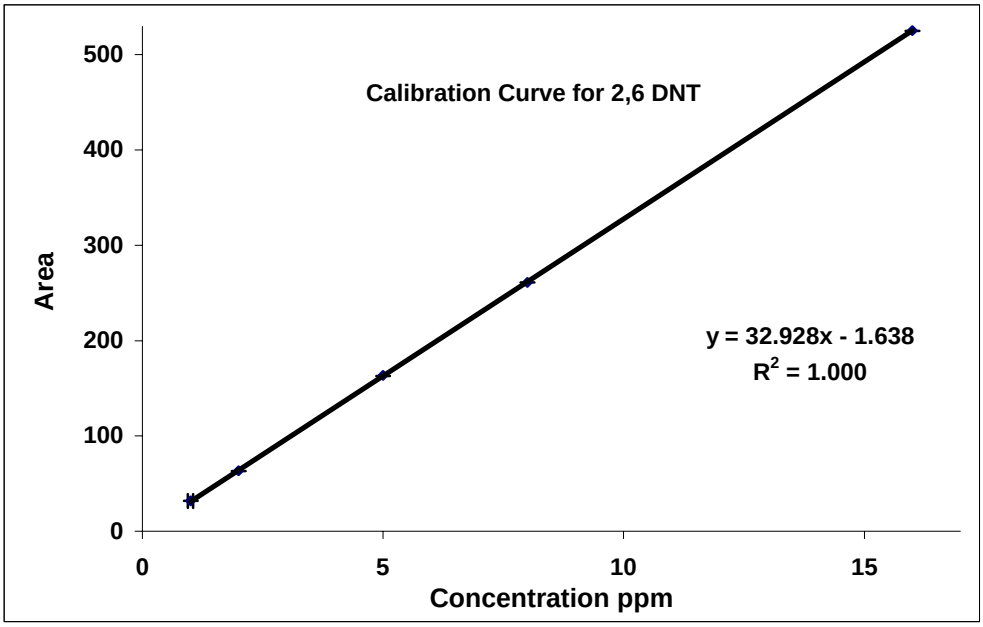

Figure A3: Calibration of curve of 2,6-DNT